Biochimica et Biophysica Acta 1808 (2011) 818–839

Contents lists available at ScienceDirect

Biochimica et Biophysica Acta

journal homepage: www.elsevier.com/locate/bbamem

Review

An NMR database for simulations of membrane dynamics

Avigdor Leftin [a], Michael F. Brown [a,b,*]

[a] Department of Chemistry, University of Arizona, Tucson, AZ 85721, USA
[b] Department of Physics, University of Arizona, Tucson, AZ 85721, USA

ARTICLE INFO

Article history:
Received 15 September 2010
Received in revised form 18 November 2010
Accepted 22 November 2010
Available online 4 December 2010

Keywords:
Cholesterol
Lipid bilayer
Lipid–protein interactions
Molecular dynamics
Nuclear spin relaxation
Order parameter
Phospholipid
Rafts
Solid-state NMR

ABSTRACT

Computational methods are powerful in capturing the results of experimental studies in terms of force fields that both explain and predict biological structures. Validation of molecular simulations requires comparison with experimental data to test and confirm computational predictions. Here we report a comprehensive database of NMR results for membrane phospholipids with interpretations intended to be accessible by non-NMR specialists. Experimental ^{13}C–^{1}H and ^{2}H NMR segmental order parameters (S_{CH} or S_{CD}) and spin-lattice (Zeeman) relaxation times (T_{1Z}) are summarized in convenient tabular form for various saturated, unsaturated, and biological membrane phospholipids. Segmental order parameters give direct information about bilayer structural properties, including the area per lipid and volumetric hydrocarbon thickness. In addition, relaxation rates provide complementary information about molecular dynamics. Particular attention is paid to the magnetic field dependence (frequency dispersion) of the NMR relaxation rates in terms of various simplified power laws. Model-free reduction of the T_{1Z} studies in terms of a power-law formalism shows that the relaxation rates for saturated phosphatidylcholines follow a single frequency-dispersive trend within the MHz regime. We show how analytical models can guide the continued development of atomistic and coarse-grained force fields. Our interpretation suggests that lipid diffusion and collective order fluctuations are implicitly governed by the viscoelastic nature of the liquid-crystalline ensemble. Collective bilayer excitations are emergent over mesoscopic length scales that fall between the molecular and bilayer dimensions, and are important for lipid organization and lipid-protein interactions. Future conceptual advances and theoretical reductions will foster understanding of biomembrane structural dynamics through a synergy of NMR measurements and molecular simulations.

Contents

Abbreviations: Chol, cholesterol; CPMG, Carr-Purcell-Meiboom-Gill; CSA, chemical shift anisotropy; DDPC, 1,2-didocosahexaenoyl-*sn*-glycero-3-phosphocholine; DLPC, 1,2-dilauroyl-*sn*-glycero-3-phosphocholine; DLPC-d_{46}, 1,2-diperdeuteriolauroyl-*sn*-glycero-3-phosphocholine; *D*, methylene travel; D_M, maximum methylene travel; DMPC, 1,2-dimyristoyl-*sn*-glycero-3-phosphocholine; DMPC-d_{54}, 1,2-diperdeuteriomyristoyl-*sn*-glycero-3-phosphocholine; DMPE, 1,2-dimyristoyl-*sn*-glycero-3-phosphoethanolamine; DMPE-d_{27}, 1-myristoyl-2-perdeuteriomyristoyl-*sn*-glycero-3-phosphoethanolamine; DOPC, 1,2-dioleoyl-*sn*-glycero-3-phosphocholine; DPPC, 1,2-dipalmitoyl-*sn*-glycero-3-phosphocholine; DPPC-d_{62}, 1,2-diperdeuteriopalmitoyl-*sn*-glycero-3-phosphocholine; DROSS, dipolar recoupling with shape and sign preservation; DSPC, 1,2-distearoyl-*sn*-glycero-3-phosphocholine; DSPC-d_{72}, 1,2-diperdeuteriostearoyl-*sn*-glycero-3-phosphocholine; GalCer, galactosylceramide; GlcCer, glucosylceramide; H_{II}, inverted hexagonal phase; MAS, magic angle spinning; MD, molecular dynamics; NMR, nuclear magnetic resonance; PC, phosphatidylcholine; PE, phosphatidylethanolamine; PLPE-d_{31}, 1-perdeuteriopalmitoyl-2-linoleoyl-*sn*-glycero-3-phosphoethanolamine; POPC, 1-palmitoyl-2-oleoyl-*sn*-glycero-3-phosphocholine; PS, phosphatidylserine; PSM, N-palmitoyl sphingomyelin; PI, phosphatidylinositol; SAXS, small-angle X-ray scattering; SLF, separated local-field

* Corresponding author. Department of Chemistry, University of Arizona, Tucson, AZ 85721, USA. Tel.: +1 520 621 2163; fax: +1 520 621 8407.
E-mail address: mfbrown@u.arizona.edu (M.F. Brown).

0005-2736/$ – see front matter © 2010 Elsevier B.V. All rights reserved.
doi:10.1016/j.bbamem.2010.11.027

Nuclear magnetic resonance spectroscopy is valuable for investigating membrane structure and dynamics because of the varied experimental techniques and multitude of probe nuclei present in the membrane. There exists a substantial and diverse body of experimental nuclear magnetic resonance (NMR) results for membrane lipid bilayers that provides important structural and dynamic information that cannot be obtained with other experimental methods [1–5]. However, for the non-specialist, NMR results may tend to be inaccessible due to their being distributed throughout the research literature, and rendered opaque by various theoretical treatments invoked in the analysis of the data [5–8]. One further aspect is that the diversity of the NMR measurements and the experimental systems studied may contribute to obscuring of the underlying general principles. Here our aim is to bring together the available experimental NMR results into a comprehensive database that is transparent to all, ranging from NMR practitioners to non-specialists in the field of molecular simulations [9–16].

1. Membrane lipids and biomembranes are liquid-crystalline materials with a hierarchy of time scales

The nature of phospholipid membrane dynamics is highlighted in this contribution, where we present and interpret NMR measurements of ^{13}C–^{1}H and ^{2}H NMR segmental order parameters and spin-lattice relaxation frequency dispersions for a comprehensive series of saturated, unsaturated, and biological phospholipid membranes. Experimental NMR methodologies and closed-form biophysical models are provided in order to demonstrate how this benchmark experimental technique enables molecular dynamics to be observed. Nuclear spin-lattice (T_{1Z}) relaxation studies show that the rates recorded as a function of magnetic field for unsaturated and saturated phosphatidylcholines follow a single frequency dispersive trend that spans the MHz regime (correlation times in the nanosecond to microsecond range). This trend suggests that experimentally determined rates of anisotropic rotational diffusion and molecular order fluctuations are determined by the viscoelastic nature of the liquid-crystalline membrane ensemble. Global perspectives from model-free and model-dependent interpretations of the comprehensive set are presented in the context of comparison to other experimental and computational methods to foster understanding of biomembrane structural dynamics.

Another of our main goals is to develop the notion of phospholipid membrane dynamics within a hierarchical framework that includes a large sampling of the experimental data sets. Interpretation of the data within the framework of a simple heuristic structural and dynamic picture involving closed-form analytical expressions allows us to illustrate general features that can be further refined through consideration of molecularly specific interactions. Various NMR studies of the structural and dynamic features of membranes are conceptualized, whereby spatial dimensions such as local segmental order, molecular orientation, and continuum geometries are considered. The temporal dimension involves the correlation times of the motions associated with the geometrical transformations of each spatial frame in accord with a hierarchy of the timescales for the various possible lipid motions.

Equilibrium and dynamical properties of membrane lipid bilayers correspond to a multi-dimensional energy landscape that may be probed with diverse biophysical techniques (cf. Fig. 1). Equilibrium properties are due to segmental, molecular, and collective fluctuations averaged over appropriate time scales, and can be explored with methods like X-ray scattering [17–20], neutron scattering [21–26], and spectroscopic techniques encompassing Fourier transform infrared [27–29] or Raman spectroscopy [30–32]. Examples of equilibrium properties for a planar membrane include the mean cross-sectional lipid area $\langle A \rangle$ and the volumetric thickness D_C, as well as the corresponding compressibility moduli such as the area (lateral) compressibility modulus k_a as discussed in the excellent reviews by Nagle and Tristram-Nagle [20,33] and Zimmerberg and Gawrisch [34]. Membrane curvature is described by the spontaneous (intrinsic) curvature H_0 and the bending modulus k_c together with the saddle (Gaussian) curvature modulus and compression modulus, and affords a means of conceptually understanding membrane deformation and lipid–protein interactions [35,36].

By contrast, dynamical properties correspond to the magnitudes and rates of fluctuations of the structural quantities about the equilibrium average, and are probed by techniques such as neutron scattering [24] and NMR relaxation [5–8,37–39]. Examples include local isomerizations of the lipid related to the microviscosity of the membrane interior, diffusional (rotational and translational) lipid motions, and collective fluctuations of the membrane. It follows from the fluctuation–dissipation theorem that the macroscopic relaxation rates are essentially manifestations of dynamical processes with contributions from mobility of the reference frames that also express the equilibrium (static) picture of the membrane. Hence, dynamics measurements in conjunction with equilibrium studies can provide a comprehensive view of the lipid properties that underlie membrane deformation and protein conformational changes [40,41], as well as membrane remodeling [42,43] and curvature sensing [35,41,44]. Further interpretation at a fundamental level in terms of molecular forces entails either simplified models that are more or less exactly solvable [45–47], or more exact models whose approximate solution requires numerical methods [9,48,49]. Knowledge of the molecular forces implicated in membrane deformation in turn can give a deeper understanding of the material properties, as well as lipid–protein interactions implicated in various key biological functions.

According to the hierarchy depicted in Fig. 1 arranged from smallest to largest time scale, we first focus on the individual C–H bonds. These segmental sites fluctuate with correlation times in the range of femtoseconds to nanoseconds due to vibrational motion, *trans–gauche* isomerizations, and restricted segmental reorientation. One step up in the temporal hierarchy, one may consider the orientational fluctuations of the lipid molecules. Anisotropic motion

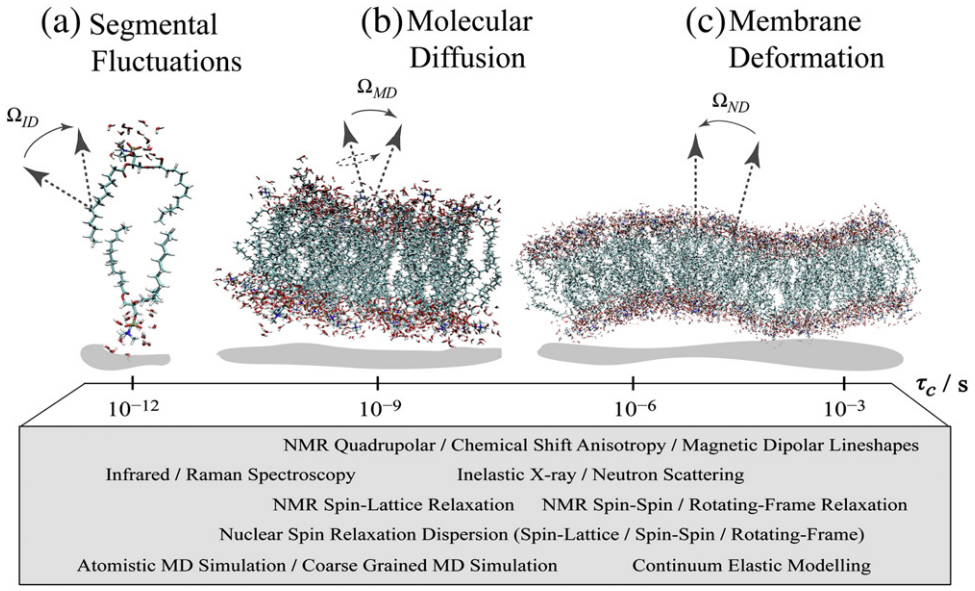

Fig. 1. NMR spectroscopy reveals phospholipid membrane dynamics and structure over a range of timescales. The energy landscape of phospholipid mobility is characterized by segmental fluctuations, molecular diffusion, and viscoelastic membrane deformation. Orientational fluctuations correspond to geometry of interactions via Euler angles Ω and by correlation times τ_c of the motions. (a) Principal axis system of ^{13}C–^{1}H or C–^{2}H bonds fluctuates due to motions of internal segmental frame (I) with respect to the membrane director axis (D). (b) Diffusive phospholipid motions are described by anisotropic reorientation of molecule-fixed frame (M) with respect to the membrane director axis (D). (c) Liquid-crystalline bilayer lends itself to propagation of thermally excited quasi-periodic fluctuations in membrane curvature expressed by motion of the local membrane normal (N) relative to membrane director axis (D). The appropriate range of timescales of various complementary biophysical methods is indicated at the bottom of the figure.

with correlation times in the range of nanoseconds to microseconds lends the molecular assembly properties of a smectic or lyotropic liquid-crystal [50,51]. Lastly, the macroscopic organization and order of lipid molecules correspond to continuum thermal viscoelastic deformations with correlation times in the range of microseconds to seconds [52,53]. These structural and dynamic features are characterized by various biophysical techniques, in particular small-angle X-ray scattering [33], molecular dynamics simulations [9], and NMR spectroscopy [5].

2. Nuclear magnetic resonance spectroscopy provides an experimental database for membrane simulations

Intermolecular forces underlie self-organization, material properties, and protein interactions of membrane lipids and are implicated in their key biological functions. Such forces are manifested through the mean-square amplitudes and rates of the lipid fluctuations described by a multi-dimensional energy landscape [54] with a hierarchy of time scales (Fig. 1). Molecular simulations capture these interactions in terms of force fields that continue to generate widespread excitement in the fields of membrane biophysics and biochemistry [9]. One of the major experimental avenues needed for validation of such molecular mechanics force fields [55] is NMR spectroscopy. Solid-state and solution NMR methods provide experimental knowledge about both the mean structure and the rates of structural fluctuations of membrane lipids. Here we describe a comprehensive database of NMR results for membrane phospholipids as summarized in the Supplementary Content of this article. We provide order parameters and NMR relaxation rates in convenient tabular form for different lipid head group types, length and degree of acyl chain unsaturation, and the presence of additives such as detergents and cholesterol. Analytical models are presented in mathematical closed form that can guide the continued development of atomistic and coarse-grained force fields. Special attention is paid to the magnetic field dependence (frequency dispersion) of the NMR relaxation rates in terms of various simplified power laws. Our results point to the influences of collective bilayer excitations that are emergent over mesoscopic length scales falling between the molecular and bilayer dimensions. Properties detected with NMR encompass a balance of forces that may be very important for membrane functions, including lipid organization, remodeling, and curvature interactions of membrane proteins, which can be further interpreted in terms of the underlying intermolecular forces through molecular simulations.

A large number of lipid bilayer types and membrane components have been subjected to NMR studies. Application of solid-state NMR methods to lipid membranes has involved the laboratories of Myer Bloom [56,57], Robert Griffin [2,58], Joachim Seelig [1,59,60], and others. The various multinuclear NMR studies of pure and multicomponent phospholipid membranes are surveyed in Table 1, which build upon the classic spin-label EPR studies of Hubbell and McConnell [61,62]. Results are classified in terms of the chemical composition of the phospholipid system, specific molecular site studied, type of nucleus observed, and experimental observable. The composition of the membranes ranges from simple fatty acids to natural biomembranes. They include the benchmark saturated phospholipid membranes, cholesterol-containing bilayers, domain-forming lipid mixtures, and lipid–protein systems. The NMR experiments are designed to localize the structural or dynamic measurements to specific sites via the various detectable nuclei in lipid membranes. The acyl chain nuclei (^{2}H, ^{13}C, ^{1}H), glycerol backbone (^{2}H, ^{13}C, ^{1}H), and headgroup (^{2}H, ^{13}C, ^{1}H, ^{31}P) regions are all detectable in the NMR experiments, either selectively by isotopic enrichment, or simultaneously by multidimensional pulse methods. The NMR observables further classify the experimental studies. One target of the experimental studies is the segmental order parameter obtained from the anisotropic solid-state ^{2}H NMR (nuclear electric quadrupolar) and ^{13}C–^{1}H (direct magnetic dipolar) lineshapes. Similarly, the chemical shift anisotropy (CSA) observed in ^{31}P NMR and ^{13}C NMR spectroscopy is useful in defining lipid orientation and phase. Isotropic chemical shifts (δ) in ^{31}P, ^{1}H, and ^{13}C NMR are indispensible NMR measurements of the phospholipid membrane. Dynamics of the system are characterized by the spin-lattice (T_{1Z}), spin–spin (T_2), and rotating frame ($T_{1\rho}$) NMR relaxation time measurements that are applicable to all nuclei. Corresponding relaxation times that provide pictures of the local properties of the molecules further characterize the motional averaging that occurs as a result of discrete and/or

Table 1
Survey of experimental NMR literature for membrane lipids and model systems.[a]

Lipid	Groups	Nucleus	Observables	Reference
Phosphatidylcholines				
Saturated	Chain, glycerol, headgroup	^{2}H	S_{CD}, T_{1Z}, T_2	[1,38,46,47,60,83,109–111,121,209]
	Chain, glycerol, headgroup	^{13}C	δ, S_{CH}, T_{1Z}	[67–69,74,75,78,107,112,124]
	Headgroup	^{31}P	CSA, T_{1Z}, T_2	[113,114,125,141,154,155,180,211–213,324]
	Chain, glycerol, headgroup	^{1}H	δ, T_{1Z}, T_2, $T_{1\rho}$	[70–72,108,115,116,145]
Unsaturated/polyunsaturated	Chain	^{2}H	S_{CD}, T_{1Z}	[92,186,189–197]
	Chain, glycerol, headgroup	^{13}C, ^{31}P	δ, CSA, S_{CH}, T_{1Z}	[188,190,201]
+ Cholesterol	Chain, glycerol, headgroup	^{2}H	S_{CD}, T_{1Z}, T_2	[80,244,251,255,263,269,270,278,309]
	Chain, glycerol, headgroup	^{1}H, ^{13}C, ^{31}P	δ, CSA, T_{1Z}, T_2	[254,257,309,314,315]
+ Detergent	Chain	^{2}H	S_{CD}, T_{1Z}	[298–305]
	Headgroup	^{31}P	CSA	[300,301,305,306]
Phosphatidylethanolamines				
Saturated/unsaturated/polyunsaturated	Chain	^{2}H	S_{CD}	[111,203–205,215,216,219,271,277]
	Headgroup	^{31}P	CSA	[206,207,212,217,218,272]
+ Cholesterol	Headgroup	^{31}P		[273–276]
Phosphatidylserines	Headgroup	^{2}H, ^{31}P	S_{CD}, CSA	[226–233]
Glycolipids	Chain, glycerol, headgroup	^{2}H, ^{13}C, ^{31}P	δ, CSA, S_{CD}, T_{1Z}	[235–238,245,246,248]
Sphingolipids	Chain, backbone, headgroup	^{2}H, ^{13}C	δ, S_{CD}, CSA	[238,240–242,244,246]
+ Cholesterol	Chain, backbone, headgroup	^{2}H, ^{13}C, ^{14}N	δ, CSA, S_{CD}	[249,252,280–282,288,289]
Natural biomembranes				
Retinal rod membranes	Chain, glycerol, headgroup	^{1}H, ^{13}C, ^{31}P	δ, CSA, T_{1Z}, T_2, $T_{1\rho}$	[316,317,319–322,327]
Sarcoplasmic reticulum membranes	Chain, glycerol, headgroup	^{1}H, ^{13}C, ^{31}P	δ, CSA, T_{1Z}	[210,324–326]
Fatty acids				
Potassium laurate	Chain	^{1}H	δ, T_{1Z}, T_2, $T_{1\rho}$	[160,165]
Potassium palmitate	Chain	^{2}H	S_{CD}, T_{1Z}	[158,161,162]
Rubidium stearate	Chain	^{2}H	S_{CD}, T_{1Z}	[163,164]
Alkanes	Chain	^{1}H, ^{13}C	δ, T_{1Z}, $T_{1\rho}$	[76,159]

[a] Symbols: CSA, chemical shift anisotropy; δ, isotropic chemical shift; S_{CD}, segmental order parameter of carbon–deuterium bond; S_{CH}, segmental order parameter of carbon–hydrogen bond; $T_{1\rho}$, nuclear spin-lattice relaxation time in the rotating-frame; T_{1Z}, nuclear Zeeman spin-lattice relaxation time; T_2, nuclear spin–spin relaxation time.

continuous phospholipid motion. When available, measurements of relaxation rates obtained at multiple magnetic fields in frequency-dispersion experiments are highlighted as well.

The following sections contain representative examples taken from the experimental literature. When possible we draw upon a comprehensive survey of currently available NMR relaxation data for membrane lipids, which is tabulated for the convenience of the reader in the Supplementary Content. A representative example of the ^{2}H and ^{13}C NMR data for the individual lipids contained in the database is presented for 1,2-dimyristoyl-*sn*-glycero-3-phosphocholine (DMPC) in Appendix A. The table columns designate the carbon positions of the lipids, and the rows correspond to the segmental order parameters (S_{CD} or S_{CH}) and nuclear spin-lattice relaxation times (T_{1Z}) for various temperatures and Larmor frequencies (magnetic fields). This presentation is adopted for the saturated, unsaturated, mixed component, and biomembrane systems in Appendix B, as discussed below.

3. Solid-state NMR spectra exhibit couplings that allow order parameters for membrane lipids to be derived

Saturated phosphatidylcholines (PC) comprise the most studied lipid systems in Table 1. NMR investigations to date have utilized the full complement of experimental methods, including lineshape measurements, relaxation time determinations, and field-dispersion relaxometry, giving information about both equilibrium and dynamical bilayer properties. Lineshape and relaxation time measurements provide a detailed picture of the structural dynamics in terms of local isomerizations that are superimposed upon continuous diffusive reorientation of the lipid molecules [63]. Introduction of variable-frequency relaxation rate measurements provides further information about membrane dynamics over a broad range, spanning segmental (fast) to collective (slow) motional regimes.

Equilibrium properties are manifested through local dynamics or structure of the phospholipid molecules as directly detected by NMR lineshapes. Nuclei such as ^{2}H, ^{13}C, ^{31}P, and ^{1}H are particularly well suited for this type of NMR measurement. This is because the spin interactions associated with each nucleus are sensitive to the orientation and motion of the phospholipids within the membrane. The interaction is determined by the type of nuclear spin coupling present in the sample. Generally, the magnetic field-dependent CSA of ^{31}P and ^{13}C nuclei, the magnetic dipolar couplings between ^{13}C–^{1}H nuclei and ^{1}H–^{1}H nuclei (D), and the nuclear electric quadrupolar interaction for deuterated lipid membranes (Q), are reflected in the corresponding anisotropic spectral lineshapes [64]. The anisotropy of the chemical shift interaction $\Delta\sigma$ is characterized in the Häberlen–Spiess convention [65] by the values of the anisotropic chemical shielding tensor σ_{ZZ}, σ_{XX}, and σ_{YY}, as $\Delta\sigma=\sigma_{ZZ}-\frac{1}{2}(\sigma_{XX}+\sigma_{YY})$ which reduces in the case of axial symmetry to $\Delta\sigma=\sigma_{\|}-\sigma_{\perp}$. The static values of the ^{13}C–^{1}H magnetic dipolar interaction, $\chi_D=(-\gamma_H\gamma_C\hbar/\pi)\langle r^{-3}\rangle$, depend on ensemble-averaged inter-nuclear distances, $\langle r^{-3}\rangle^{-1/3}$, and magnetogyric ratios (γ_C and γ_H) of the nuclei. The static coupling constant for the electric quadrupolar interaction $\chi_Q=e^2qQ/h$ is determined by the principal value of the electric field gradient tensor eq within the principal axis system of the carbon–deuterium bond, and Q is the quadrupole moment of the deuteron.

Averaging of the static interactions yields *residual dipolar couplings* (RDCs) and *residual quadrupolar couplings* (RQCs) that are directly measured from the peak-to-peak splitting $\Delta\nu_\lambda$ of the magnetic dipolar ($\lambda=D$) or electric quadrupolar ($\lambda=Q$) lineshape [66], as shown in Figs. 2(a) and (b) respectively for DMPC membranes. Through the relation $\Delta\nu_\lambda\propto\chi_\lambda S_\lambda$ the segmental order parameter $S_\lambda\equiv\langle P_2(\cos\beta)\rangle=\frac{1}{2}\langle 3\cos^2\beta-1\rangle$ may be calculated, allowing the residual coupling to be quantified for a given ensemble-averaged orientation of a specific segmental site. High-resolution NMR measurements of isotropic chemical shifts may be augmented by two-dimensional separated

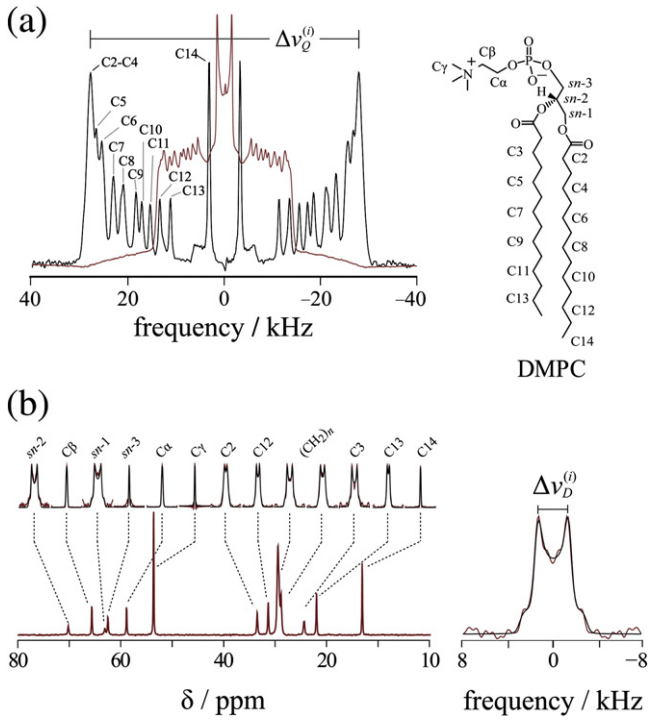

Fig. 2. Solid-state NMR provides residual quadrupolar couplings (RQCs) and residual dipolar couplings (RDCs) that directly correspond to ensemble-averaged molecular structure. (a) The ^{2}H NMR quadrupolar powder-pattern spectrum (light red line) exhibits axial symmetry characteristic of the liquid-crystalline phase for DMPC at 30 °C. Numerically deconvoluted (de-Paked) ^{2}H NMR spectrum (dark line) reveals quadrupolar splittings $\Delta\nu_Q^{(i)}$ for individual methylene segments (i) of acyl chains. (b) Isotropic ^{13}C chemical shifts (δ) and pseudostatic recoupled anisotropic powder patterns are obtained under ^{13}C–^{1}H magic-angle spinning (MAS) using the separated local-field (SLF) pulse sequence DROSS [67]. The solid-state ^{13}C–^{1}H lineshapes reveal magnetic dipolar splittings $\Delta\nu_D^{(i)}$ for each of the resolved chemically-shifted resonances. The chemical structure of DMPC and spectral assignments are shown.

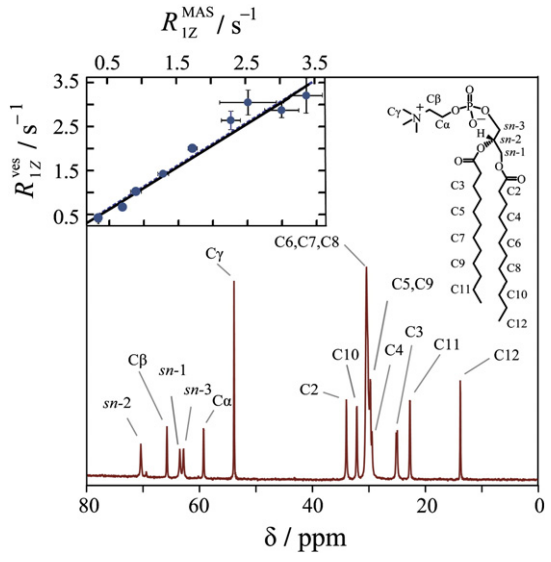

Fig. 3. High-resolution solid-state ^{13}C NMR spectroscopy of membrane lipids reveals chemical shifts and nuclear spin-lattice (R_{1Z}) relaxation rates. Isotropic ^{13}C NMR chemical shift (δ) frequency spectrum obtained under magic-angle spinning (MAS) conditions (6 kHz ± 2 Hz, SPINAL-64 ^{1}H-decoupling field strength of 50 kHz) for multilamellar DLPC vesicle dispersion at 30 °C. Inset depicts nuclear spin-lattice relaxation rates (R_{1Z}) for $(CH_2)_n$ carbons (C4–C11) obtained for small unilamellar vesicles (ves) under stationary high-resolution solution NMR conditions versus those for multilamellar dispersions using solid-state MAS techniques. The molecular structure of DLPC and assignments corresponding to the chemical shift assignments in the ^{13}C NMR spectra are shown.

local field (SLF) measurements that allow the simultaneous determination of chemical shift spectra (direct frequency dimension, ν_2), and powder-type lineshapes (indirect frequency dimension, ν_1) for all resolved segmental positions under magic-angle spinning (MAS) conditions [67–69]. These segmental order parameters may be found tabulated for various membranes in Appendix A and in the Supplementary Content.

Motions much faster than the static coupling result in isotopic frequency spectra, such as the ^{13}C chemical shift spectrum of 1,2-dilauroyl-*sn*-glycero-3-phosphocholine (DLPC) obtained using MAS shown in Fig. 3. These high-resolution experiments report on the acyl chain, backbone, and head group regions simultaneously at multiple nuclear sites at natural isotopic abundance. The ^{13}C isotropic chemical shifts in the MAS experiment are similar to those recorded under comparable solution-phase conditions [70–77]. Furthermore, the *spin-lattice relaxation rates* (R_{1Z}) of multilamellar lipids measured with solid-state NMR methods and small unilamellar vesicles measured with solution-state NMR are nearly identical (Fig. 3, inset). This similarity has been reproduced in recent studies where the NMR relaxation times of small vesicles and vesicle dispersions have been compared through Brownian dynamics simulations that demonstrate the influence of torsional potentials on the dynamics of the bilayer lipids [78]. The extended data sets presented in the database offer an opportunity to compare the magnetic field (Larmor frequency) dispersions of ^{13}C NMR relaxation rates for multiple saturated and unsaturated lipids, thus allowing simulation comparisons invoking multiple time scales.

Early investigations [1,79,80] utilized site-specific labeling strategies, whereby synthetically accessible C–H sites along the acyl chain of the molecule, the glycerol backbone, and choline headgroup were replaced by C–^{2}H bonds. These ^{2}H NMR studies revealed a systematic variation of the lineshapes as a function of segmental position, due to variations in the degree of motional averaging. Each site exhibits symmetric powder-type lineshapes, i.e. quadrupolar Pake doublets, reduced in peak-to-peak splitting from the static values expected for rigid segments. At these segmental sites, the RQCs are large at the upper region of the acyl chain, and decrease progressively toward the distal end of the chain [81–83]. A statistical treatment based on the Flory rotational isomeric model [84] or Marčelja mean-field treatment [85] can reproduce the residual quadrupolar ^{2}H NMR lineshape scaling [86–92]. This approach combines chain statistics which manifest the probabilities of *gauche* (g) and *trans* (t) segmental conformations confined to allowed sites in a discrete diamond-lattice, together with axially anisotropic rotations of the phospholipid about the membrane normal. Such a combined experimental and modeling approach has led to the widespread application of measurements of the carbon–deuterium segmental order parameter S_{CD}, and more recently of the carbon–hydrogen segmental order parameter S_{CH} in membranes.

Moreover, extensive studies making use of perdeuteration of the carbon acyl chains have yielded comprehensive benchmark measurements of S_{CD} values for the homologous series of saturated phosphatidylcholines in the literature [47,93–96]. Use of acyl-perdeuterated lipids allows the investigation of a far greater number of sites in lipid systems than are accessible with specifically deuterated lipid systems. Analysis of the segmental order parameters—in conjunction with statistical models—yields average cross-sectional areas and membrane volumetric thicknesses that are similar to those measured from small-angle X-ray scattering (SAXS) experiments and neutron scattering experiments of membranes [26]. The geometrical picture of phospholipid membranes from NMR is complementary to that of the scattering experiment. A difference is that NMR reports specifically on each lipid segment site via the ensemble-averaged segmental order parameter, while differences in electron density in X-ray (phosphate versus hydrocarbon and water), or neutron density (protiated versus deuterated) in related scattering experiments are detected. In the NMR picture,

Table 2
Calculation of phospholipid bilayer structural properties for mean-torque model.[a]

Cross-sectional area per lipid[b]
$\langle A\rangle = 2\langle A_C\rangle = 4V_{CH_2}q / D_M$
Volumetric thickness per monolayer
$D_C = n_C D_M / 2q$
Area factor
$q \equiv \langle \cos\beta^{-1}\rangle \approx 3 - 3\langle\cos\beta\rangle + \langle\cos^2\beta\rangle$
Moments of orientational distribution
$\langle\cos\beta\rangle = \coth(-U_1/k_BT) + k_BT/U_1 = \frac{1}{2}(1 + \sqrt{(-8S_\lambda - 1)/3})$
$\langle\cos^2\beta\rangle = 1 + 2(k_BT/U_1)^2 + 2(k_BT/U_1)\coth(-U_1/k_BT) = \frac{1}{3}(1-4S_\lambda)$

[a] Symbols: $\langle A\rangle$, mean cross-sectional area per lipid; $\langle A_C\rangle$, mean cross-sectional area per acyl chain; β, orientational angle; D_C, volumetric hydrocarbon thickness per monolayer; D_M, maximum methylene travel; k_B, Boltzmann constant; n_C, number of carbon segments; q, area factor; S_λ, generalized segmental order parameter; T, temperature; U_1, first-order mean-torque potential energy; V_{CH_2}, methylene volume. Additional details may be found in Ref. [47].

[b] Maximum methylene travel projection of all-*trans* rigid segment is $D_M = 2.54$ Å as defined by vector connecting C($i+1$)−C($i-1$) carbons projected onto membrane normal.

each site of deuteration corresponds to a given carbon position and is assigned an index designation *i*. In the database tables, for example, the benchmark DMPC lipid bilayer has number of carbons $n_C = 14$ in the acyl chain, where $i = 2\ldots13$ corresponds to the individual methylene segments, such that $i = 14$ is the deuterated terminal methyl group. This convention is adopted for the ^{2}H and ^{13}C NMR entries for acyl chains in the database, while additional notation is used when needed for backbone and headgroup sites.

The molecular order parameter is related to the average orientation of the *i*th methylene carbon defined by the projection of the vector (virtual bond) connecting the $i+1$ and $i-1$ methylene carbons onto the bilayer normal (director axis) through the deflection angle β. The value of the average methylene projection, or travel (D) along the bilayer normal, is given with respect to the all-*trans* maximum methylene travel value ($D_M = 2.54$ Å) by $D = D_M\langle\cos\beta\rangle$. Using the equilibrium averages calculated from the Boltzmann orientational distribution within a mean-field (mean-torque) orientational potential, the methylene projection may be determined from the measured segmental order parameter [97]. Following a simple expansion of the orientational distribution, the hydrocarbon thickness per monolayer D_C and average cross-sectional area per lipid $\langle A\rangle$ are calculated from the methylene projection. The analytical expressions allowing these structural quantities to be determined are summarized in Table 2 [47,97]. The results from the application of the mean-torque model to the NMR segmental order parameters for each of the lipids for the homologous saturated phosphatidylcholine series in the liquid-crystalline (L_α) state are shown in Fig. 4. These measures are useful quantities for starting geometries of dynamics simulations [98]. Numerical results are presented beside the plateau order parameters (S_{plat}) for the lipids in Table 3. The values of the order parameter are largest near the L_α to L_β phase transition, where acyl chain lengths approach the all-*trans* segmental limit. At intermediate temperatures, for instance 10 °C above the phase transition of a specific lipid, cross-sectional areas are smallest for DLPC (56.7 Å^2) and largest for 1,2-distearoyl-*sn*-glycero-3-phosphocholine (DSPC) (66.0 Å^2). This suggests that the statistical degrees of freedom for the chain travel, at a given distance from the order–disorder phase transition, is sensitive to contributions from chain length, where bilayer mid-plane segments experience the smallest mean-torque restoring potential compared with upper acyl segments.

The sensitivity of the acyl chain order parameters to local segmental environment is the premier reason for targeting this structural parameter in both experiment and simulation. In ^{2}H NMR experiments this allows for local probes of all isotopically enriched carbon sites. For ^{13}C–^{1}H recoupling experiments, site-resolved probes of lipid structure are obtained at all ^{13}C sites at natural isotopic abundance. It is not known *a priori* what constrains the fluctuations of

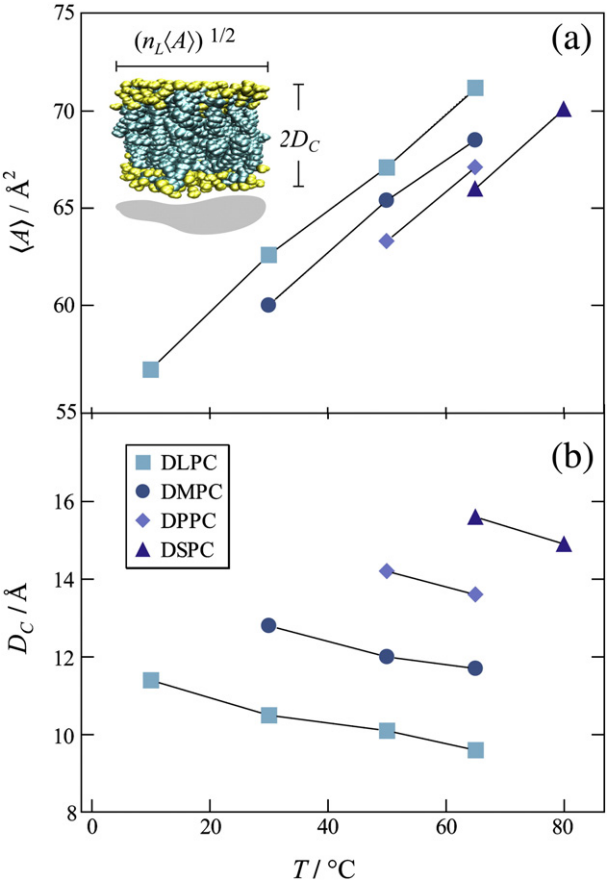

Fig. 4. Structural parameters for liquid-crystalline membranes are derived from ^{2}H NMR spectral data by applying a simple mean-torque model. Properties of membranes include the hydrocarbon thickness D_C and cross-sectional area per lipid $\langle A\rangle$. (a) Variation of the average cross-sectional areas $\langle A\rangle$ are shown for (■) DLPC, (●) DMPC, (◆) DPPC, and (▲) DSPC at temperatures of 10, 30, 50, 65, and 80 °C using data from Ref. [47]. (b) Hydrocarbon thickness per monolayer D_C for homologous saturated phosphatidylcholines shows reduction with increasing temperature for the data set as in (a). Inset depicts the structural parameters of a phospholipid bilayer with number of lipids n_L and total volume given by $2n_L\langle A\rangle(D_C + D_H)$, where D_H is the headgroup thickness. Phospholipid membrane graphics generated with CHARMM-GUI [98].

the segments—yet membrane composition greatly affects the observed values. The dynamics simulations can access all order parameters for all sites given appropriate potential parameterization. This constitutes a challenge for simulations targeting cross-sectional

Table 3
Structural results for saturated phospholipids determined from residual coupling interactions.[a,b]

Lipid	T/°C	S_{plat}	D_C/Å	$\langle A\rangle$/Å^2
DLPC	10	0.229	11.4	56.7
	30	0.193	10.5	62.6
	50	0.175	10.1	67.1
	65	0.160	9.60	71.2
DMPC	30	0.213	12.8	60.0
	50	0.184	12.0	65.4
	65	0.173	11.7	68.5
DPPC	50	0.198	14.2	63.3
	65	0.181	13.6	67.1
	80	0.163	13.0	71.9
DSPC	65	0.188	15.6	66.0
	80	0.171	14.9	70.1

[a] Symbols: $\langle A\rangle$, average cross-sectional area per lipid; D_C, volumetric hydrocarbon thickness per monolayer; S_{plat}, plateau order parameter; T, temperature.

[b] Data from Ref. [47].

areas that must balance parameterization of the force-field with accuracy of the numerical treatment of the analytically determined structural and dynamic results [99–101]. The reduction of orientational freedom of the segments can be achieved by adjusting ensemble size, as well as periodic boundary conditions important for the force-field of the simulation environment, without changing the physical composition of the bilayer. Additionally, torsional potentials must be specifically accounted for in the case of the glycerol backbone. For example, in the ^{2}H NMR experiment one observes inequivalent deuterons of the *sn*-2 C2 position and *sn*-1 and *sn*-2 acyl upper chain segments [60]. This is due to orientation as well as packing of lipid glycerol groups that are important aspects of simulations. By fine-tuning the allowed torsional rotations of the glycerol backbone and chains, excellent correspondence between NMR and MD order parameters have been demonstrated at this benchmark site of comparison [102].

4. NMR relaxation gives dynamical parameters that characterize membrane lipid motions and bilayer fluctuations

Studies of membrane structural dynamics involve measurement of nuclear spin relaxation rates that introduces the fourth dimension of time marking the fluctuations of the system [57]. In general, the relaxation depends on the mean-squared amplitudes and rates of the motions [103]. The mean-squared amplitudes are expanded in a Clebsch–Gordon series in terms of the order parameters (second- and fourth-rank) [8]. The relaxation depends not only on the geometry but also the correlation times for the motions [104,105]—such measurements allow the time constants associated with the structural dynamics of the membrane to be established. Refinement of the experimental data is performed against dynamic models, whereby the ensemble-averaged fluctuations are characterized by the mean-square amplitudes and the correlation times of the motions according to Redfield theory [106]. The NMR signals are sensitive to the power spectra of the motional fluctuations at characteristic frequencies. For Zeeman nuclear spin-lattice (T_{1Z}) relaxation, the dynamics of the membrane are explored on a timescale from picoseconds to milliseconds, as measured relative to the inverse of the nuclear Larmor frequency (proportional to the magnetic field strength). Analogously, for spin-lattice relaxation in the rotating frame ($T_{1\rho}$), the relaxation rates contain contributions (μs to ms) to the time scale of the dynamics that correspond to the inverse of the lower frequency, time-dependent magnetic field used to detect the NMR signal. Lastly, for spin-echo measurements, the timescale of the spin-spin relaxation (T_2) is the inverse of the radio-frequency pulse repetition rate (ns to ms). Motions on these time scales modulate the nuclear spin Hamiltonian that govern the relaxation times, and allow motions over a broad range of timescales to be monitored. The contributions from local segmental fluctuations and order fluctuations due to molecular reorientations in a mean-field potential or bilayer collective motions are further considered below.

Segmental dynamics may be probed in a site-specific manner by measuring the relaxation times for all the chemically-shifted peak positions in the NMR spectrum. Early investigations utilizing high-resolution ^{1}H NMR and natural-abundance ^{13}C NMR measurements identified differences of T_{1Z} times for various regions of the lipid [70–73,75,107,108]. Hydrocarbon acyl chain T_{1Z} values were shown to increase sharply towards the interior of the membrane, while smaller values were observed at the glycerol interface. Choline headgroup relaxation times were also observed to be large compared to the upper acyl chain and glycerol backbone. However, since the relaxation rates and spectral densities depend on both the amplitude and the rate of the motion, *a priori* one cannot say whether the relaxation profile is due to accumulation of the motional rate along the chain, or rather a decrease in segmental ordering approaching the bilayer center [109]. Nonetheless, in early work the T_{1Z} data were interpreted in terms of a gradient of the motional rates increasing from the glycerol backbone towards either the polar headgroup or hydrocarbon region of the bilayer [75].

The measurement of T_{1Z} is useful for determining correlation times τ_c on the order of picoseconds to microseconds, while the T_2 measurement reports on ranges from nanoseconds to milliseconds. The temperature dependence of these NMR experiments is an important parameter, because both the Boltzmann distribution of order parameters and the Arrhenius dependence of the relaxation rates may be revealed by the trends in relaxation times in these regimes [8]. A comprehensive set of temperature-dependent T_{1Z} values has been reported for DMPC specifically deuterated at the C2, C6, C13, and C14 positions of the acyl chain [38]. Both intermolecular segmental isomerization and the intra-molecular anisotropic mean-field ordering potential have been considered through fitting to multiple reorientational correlation times. From these correlation times of motion, and the temperature dependence of the relaxation times, energetic barriers for the anisotropic rotational motion of the lipid molecules were determined, and barriers for segmental isomerizations have been identified at the isotopically enriched sites probed in the experiment. The energetic barrier for overall lipid reorientation was found to be on the order of that determined for the upper acyl chain positions. Further, the energy barriers were found to decrease progressively towards the distal end of the acyl chain. This anisotropy in the activation energy values suggests that the acyl chains of the lipid are relatively free to reorient in the center of the membrane, while they are constrained at the aqueous interface, giving rise to a wobble-in-a-cone type motional distribution. The numerical results parallel the observations made in similar multinuclear studies combining T_{1Z} and lineshape measurements, with temperature being an additional experimental variable [110–116].

An additional NMR technique—following from early pioneering work of Friedrich Noack in the field of liquid crystals and polymers [117]—is the relaxation rate-frequency dispersion measurement. Variation of the Larmor frequency (magnetic field) in the T_{1Z} experiment, or pulse repetition rate in the $T_{2\mathrm{CPMG}}$ (CPMG, Carr–Purcell–Meiboom–Gill) [118,119] experiment, provides an experimental variable that is useful for testing motional models according to the frequency dependence of the spectral densities of motion [115,120,121]. Here, spin-lattice relaxation rates recorded as a function of Larmor frequency (field strength) enable one to test specific dynamic models [122,123]. The dynamics contributing to this scaling have been shown in extensive ^{2}H and ^{13}C NMR relaxation studies to depend on segmental, molecular, and mesoscopic, i.e. collective dynamic processes [8]. There has recently been resurgence in the application of this technique in the field of membrane biophysics, whereby high-resolution ^{31}P NMR and ^{13}C NMR have been used by Redfield and coworkers to extract dynamic parameters for small phospholipid vesicles [124–126]. Moreover, this technique is used extensively in the study of proteins that continue to extend the view of these dynamic systems [127–132].

A ^{13}C NMR rate profile measured using this field dispersion technique is shown in Fig. 5 for the benchmark saturated phosphatidylcholine 1,2-dipalmitoyl-*sn*-glycero-3-phosphocholine (DPPC), constructed using ^{13}C NMR data found in the Supplementary Content. At the terminus of the acyl chain region, the smallest relaxation rates are observed for the C14, C15 methylene segments and terminal CH_3 group. The rate is little affected by changes in magnetic field, suggesting that the motion of this region of the lipid membrane is much faster than the inverse of the Larmor frequency. Continuing along the acyl chain, the experimental limitation of spectral resolution results in the characteristic plateau region of the rate profile, where resonances of like chemical shift become indistinguishable from one another. For all saturated phosphatidylcholines, in the ^{13}C NMR relaxation experiment spectral overlap exists for the $(CH_2)_n$ carbon

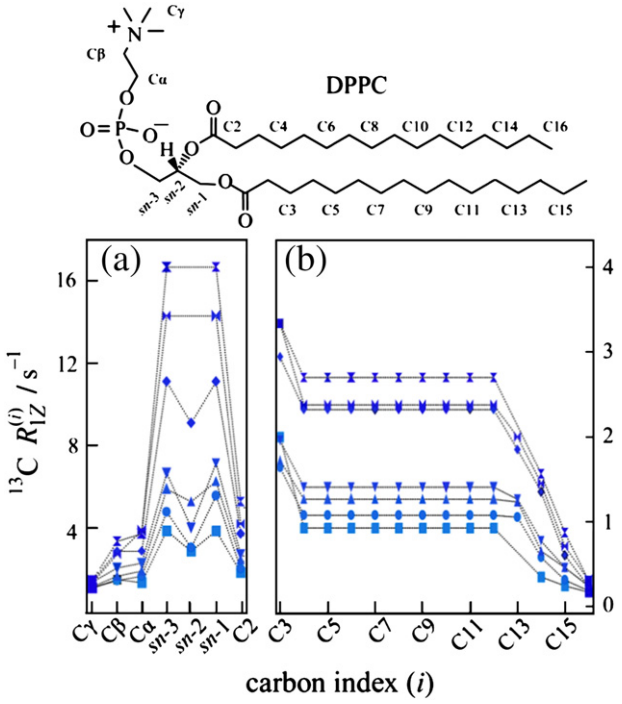

Fig. 5. High-resolution ^{13}C NMR spin-lattice relaxation rate profiles for liquid-crystalline DPPC show a significant frequency dispersion characteristic of a motional hierarchy. Spin-lattice relaxation rates $R_{1Z}^{(i)}$ are presented for various carbon positions (i) of DPPC at 50 °C at Larmor frequencies of (⧗) 15.04 MHz, (◗) 20.00 MHz, (♦) 25.15 MHz, (▼) 45.29 MHz, (▲) 90.80 MHz, (●) 125.76 MHz, and (■) 150.84 MHz. (a) The glycerol backbone and choline headgroup are resolved in natural-abundance ^{13}C NMR in the 50–80 ppm region and exhibit a pronounced dispersion of the relaxation rates. (b) Acyl chain segments are observed in the 0–40 ppm fingerprint region of the high-resolution ^{13}C NMR spectrum. The molecular structure of DPPC and assignments corresponding to the carbon index (i) are shown. Data taken in part from Ref. [96].

resonances (C4 to C11) at the center region of the acyl chain, while in the complementary ^{2}H NMR experiment the upper acyl chain region, C2 to C6–C8, is usually contained within the plateau region. In this region, for the ^{13}C sites the reduction in magnetic field results in an increase in relaxation rate, reflecting the contributions from motions on the order of or slower than the inverse of the Larmor frequency. For the ^{13}C NMR results, the relaxation rate at the C3 position rate is larger than the plateau region, and the C2 rate increases with respect to both C3 and the plateau carbons. The scaling of the relaxation rate similarly increases towards the interfacial hydrocarbon region. In Fig. 5(a) this trend in increasing relaxation rates in the profile continues into the glycerol backbone region (*sn*-1, *sn*-2, *sn*-3) of the lipid. Here relaxation rate dispersions are most sensitive, and are over four times as large as for the acyl chain relaxation rates. In Fig. 5(b) the choline Cα, Cβ rates are reduced compared to the glycerol backbone region, and are on the order of the C2 and C3 acyl chain relaxation rates. The Cγ rate is at an intermediate value, lower than the upper acyl chain region, but larger than the terminal region of the lipid acyl chain, again reflecting fast rotational motion and isomerization. This relaxation rate-dispersion profile is a useful tool for inspection of site-distributed dynamics of the lipid bilayer.

5. Analytical theories are valuable complements to molecular simulations of lipid bilayers

5.1. Model-free aspects of membrane dynamics

Reduction and analysis of the experimental data ultimately involve the introduction of dynamic models. Microscopic motional models may be constructed through parameterization of the total energy of the system in terms of the amplitude and frequency of the various fluctuation modes of the membrane. There are basically two conceptual avenues that can be taken—which are not exclusive—to parameterization of these rate expressions. First, we can introduce simplified models in analytical, mathematical closed-form, with the advantage they can be solved easily and exactly. Second, we can introduce more realistic and complex models, whose force fields require approximate, numerical solution. In either case, ultimately one would like to establish the correspondence to properties of the membrane lipid bilayer. From the vantage point of the experimentalist, the power spectral densities $J_m(\omega)$ of the modes are formulated in terms of their contributions to segmental, molecular, and collective membrane dynamics. The functional form of the rate expressions and their dependence on the spectral densities is presented in Table 4 [5,63]. From simple fitting to power-law generalizations, this formalism may be used as a means to assess the motional contributions to experimental data, and may guide the approximate force-field models by suggesting relative contributions to simulation potentials.

Table 4
Expressions for the calculation of phospholipid bilayer structural dynamics[a].

Anisotropic nuclear spin coupling[b,c]
$\Delta\nu_\lambda = \Delta\nu_\lambda^{\|} \sum_n D_{0n}^{(2)}(\Omega_{PD}) D_{n0}^{(2)}(\Omega_{DL})$
Homonuclear (^{2}H) nuclear spin-lattice relaxation rate
$R_{1Z}(\omega_D) = 1/T_{1Z} = \frac{3}{4}\pi^2\chi_Q^2[J_1(\omega_D) + 4J_2(2\omega_D)]$
Heteronuclear (^{13}C–^{1}H) nuclear spin-lattice relaxation rate
$R_{1Z}(\omega_C) = 1/T_{1Z} = \frac{3}{2}N_H\pi^2\chi_D^2[\frac{1}{6}J_0(\omega_H-\omega_C) + \frac{1}{2}J_1(\omega_C) + J_2(\omega_H+\omega_C)]$
Spectral density of motion
$J_m(\omega) = \mathrm{Re}\int_{-\infty}^{\infty} G_m(t)e^{-i\omega t}dt$

[a] Symbols: χ_λ, generalized anisotropic coupling constant; $\Delta\nu_\lambda$, generalized anisotropic lineshape splitting; $\Delta\nu_\lambda^{\|}$, maximum splitting for interaction principal axis parallel to the main magnetic field ($\Delta\nu_Q^{\|} = \frac{3}{2}\chi_Q$, $\Delta\nu_D^{\|} = \chi_D$); $D_{n'n}^{(j)}(\Omega)$, Wigner rotation matrix element of rank j and projection indices (n',n); $G_m(t)$, time-dependent correlation function ($m=0,1,2$); $J_m(\omega)$, frequency-dependent power spectral density of motion; λ, generalized anisotropic coupling interaction ($\lambda = D \equiv$ dipolar, $\lambda = Q \equiv$ quadrupolar); N_H, number of hydrogens directly bonded to ^{13}C atom; R_{1Z}, nuclear Zeeman spin-lattice relaxation rate; T_{1Z}, nuclear Zeeman spin-lattice relaxation time; ω_C, carbon Larmor frequency; ω_D, deuteron Larmor frequency; ω_H, hydrogen Larmor frequency; Ω, Euler angles (α,β,γ). Additional details may be found in Ref. [5].

[b] Euler angle indices correspond to principal axis system (P), director frame (D), and laboratory frame (L).

[c] Wigner rotation matrix elements $D_{n'n}^{(j)}(\Omega)$ are related to the (associated) Legendre polynomials by $D_{n'n}^{(j)}(\alpha,\beta,\gamma) = e^{-in'\alpha}(-1)^{n'}\sqrt{(j-n')!/(j+n')!}\ P_j^{n'}(\cos\beta)e^{-in\gamma}$ where $P_j^0(\cos\beta) = P_j(\cos\beta)$.

5.2. Examples of simple closed-form analytical models

Quantitative determination of the correlation times of motions from such an experimental data set is possible by using specific motional models, such as those presented in Table 5. At this level of analysis, reorientational correlation times corresponding to the $D_{\|}$ and $D_{\perp}$ values of the molecular diffusion tensor have been measured in ^{2}H NMR variable frequency T_{1Z} experiments [46,133]. These results are obtained by comparative fitting to multiple models that include mean-field potentials of even or odd symmetry, as well as contributions to the dynamics that arise from vesicle tumbling and continuum deformation [134,135] based on the classic work of Pier-Luigi Nordio [136] and Jack Freed [137]. Semi-logarithmic plots of ^{2}H NMR and ^{13}C NMR relaxation measures are shown in Fig. 6 for the rate-frequency dispersion of DMPC measured at the $(CH_2)_n$ (carbons C4–C11) and C7 segmental positions from ^{13}C NMR and ^{2}H NMR experiments, respectively. Notably, over the MHz frequency range an essentially continuous dispersion of the relaxation data is evident. These positions exhibit similar segmental order parameters, and the comparative fitting from segmental, molecular, and

Table 5
Expressions for the spectral densities of motion for dynamic models[a,b,c].

Segmental diffusion model[d]

$$J_m(\omega) = \sum_{n'}\sum_{n}\left|D^{(2)}_{0n'}(\Omega_{PI}) - (\eta_\lambda/\sqrt{6})\left[D^{(2)}_{-2n'}(\Omega_{PI}) + D^{(2)}_{2n'}(\Omega_{PI})\right]\right|^2 F^{(2)}_{n'n}(\omega,\Omega_{ID})\left|D^{(2)}_{nm}(\Omega_{DL})\right|^2$$

$$F^{(2)}_{n'n}(\omega,\Omega_{ID}) = [\langle|D^{(2)}_{n'n}(\Omega_{ID})|^2\rangle - |\langle D^{(2)}_{n'n}(\Omega_{ID})\rangle|^2\delta_{n'0}\delta_{n0}]j^{(2)}_{n'n}(\omega,\Omega_{ID})$$

Molecular diffusion model (non-collective)[d]

$$J_m(\omega) = \left|\langle D^{(2)}_{00}(\Omega_{PI})\rangle\right|^2\sum_{n'}\sum_{n}\left|D^{(2)}_{0n'}(\Omega_{IM}) - (\eta_\lambda/\sqrt{6})\left[D^{(2)}_{-2n'}(\Omega_{IM}) + D^{(2)}_{2n'}(\Omega_{IM})\right]\right|^2 \times F^{(2)}_{n'n}(\omega,\Omega_{MD})\left|D^{(2)}_{nm}(\Omega_{DL})\right|^2$$

$$F^{(2)}_{n'n}(\omega,\Omega_{MD}) = [\langle|D^{(2)}_{n'n}(\Omega_{MD})|^2\rangle - |\langle D^{(2)}_{n'n}(\Omega_{MD})\rangle|^2\delta_{n'0}\delta_{n0}]j^{(2)}_{n'n}(\omega,\Omega_{MD})$$

Flexible surface model (2D collective)[e]

$$J_m(\omega) = \tfrac{1}{2}\left|\langle D^{(2)}_{00}(\Omega_{PN})\rangle\right|^2\sum_{n=\pm1}F^{(2)}_{0n}(\omega,\Omega_{ND})\left|D^{(2)}_{nm}(\Omega_{DL})\right|^2$$

$$F^{(2)}_{0n'}(\omega,\Omega_{ND}) = C'|\omega|^{-1}$$

Membrane deformation model (3D collective)[f]

$$J_m(\omega) = \tfrac{1}{2}\left|\langle D^{(2)}_{00}(\Omega_{PN})\rangle\right|^2\sum_{n=\pm1}F^{(2)}_{0n}(\omega,\Omega_{ND})\left|D^{(2)}_{nm}(\Omega_{DL})\right|^2$$

$$F^{(2)}_{0n}(\omega,\Omega_{ND}) = C|\omega|^{-1/2}$$

[a] Symbols: C, viscoelastic factor for 3D director fluctuations; C', viscoelastic factor for 2D director fluctuations; $D^{(j)}_{n'n}(\Omega)$, Wigner rotation matrix element of rank j and projection indices (n',n); $F^{(2)}_{n'n}(\omega,\Omega)$, Fourier transform of second-rank correlation function; $j^{(2)}_{n'n}(\omega,\Omega)$, reduced second-rank power spectral density; $J_m(\omega)$, frequency-dependent power spectral density of motion; η_λ, generalized asymmetry parameter. Further details may be found in Ref. [135].

[b] Euler angle indices correspond to principal axis (P), internal segmental frame (I), molecular frame (M), local membrane frame (N), director frame (D), and laboratory frame (L).

[c] Wigner rotation matrix elements $D^{(j)}_{n'n}(\Omega)$ are related to (associated) Legendre polynomials by $D^{(j)}_{n'n}(\alpha,\beta,\gamma) = e^{-in'\alpha}(-1)^n\sqrt{(j-n')!/(j+n')!}\;P^{n'}_j(\cos\beta)e^{-in\gamma}$ where $P^0_j(\cos\beta) = P_j(\cos\beta)$.

[d] Asymmetry parameter for quadrupolar ($\lambda = Q$) and dipolar ($\lambda = D$) interactions is defined by $\eta_\lambda \equiv -\sqrt{6}\langle D^{(2)}_{0\pm2}(\Omega_{PI})\rangle / D^{(2)}_{00}(\Omega_{PI}) \approx 0$.

[e] 2D viscoelastic factor is $C' = k_BT/2K$ where k_B is Boltzmann constant and K is elastic constant.

[f] 3D viscoelastic factor is given by $C = k_BT\sqrt{\eta}/\pi\sqrt{2K^3}$ where η is viscosity.

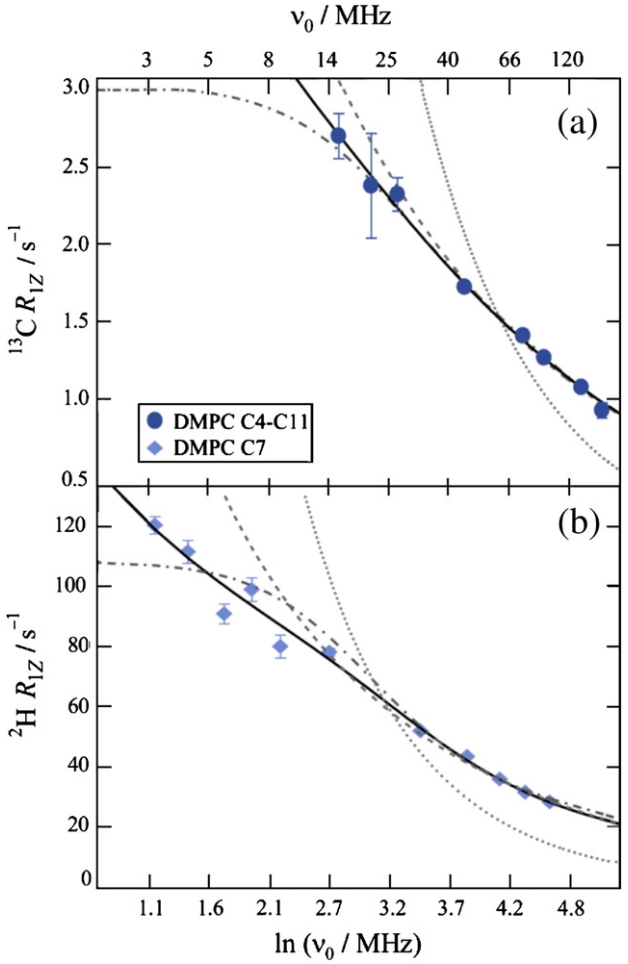

Fig. 6. Frequency dispersion of ^{13}C NMR and ^2H NMR spin-lattice relaxation rates for liquid-crystalline DMPC bilayers. Nuclear resonance frequencies for ^{13}C or ^2H nuclei at a given value of the magnetic field are indicated by $\nu_0 = \omega_0/2\pi \equiv \nu_C$ or ν_D, respectively. Non-exponential relaxation is evident by comparative fitting of models for intrinsically distributed phospholipid dynamics within the membrane bilayer. (a) ^{13}C NMR relaxation dispersion for (●) $(CH_2)_n$ carbons (C4–C11) of DMPC ($\nu_0 = 15$–150 MHz), and (b) ^2H NMR relaxation dispersion for (♦) selectively deuterated C7 carbons of 1,2[7′, 7′-^2H] DMPC ($\nu_0 = 3$–95 MHz) at 30 °C. By combining the two rate dispersions the frequency range is expanded and a simultaneous best fit is obtained using a composite membrane deformation model (——). Alternatives include molecular diffusion model (– • –), 2D flexible surface model (smectic deformation) (• • •), and (nematic-like) 3D membrane deformation model (– – –). For the composite membrane deformation model, molecular motion is described by principal values $D_{||} = 1.60\times10^8\ s^{-1}$ and $D_\perp = 2.62\times10^6\ s^{-1}$ of the anisotropic rotational diffusion tensor. Orientational fluctuations of the lipid with respect to the time-averaged membrane normal are described by $|S_{slow}| = 0.89$ yielding $\beta_{MD} \approx 16°$. The viscoelastic constant for bilayer dynamics is $C = 2.16\times10^{-6}\ s^{-1/2}$. Data taken in part from Refs. [46,96].

collective membrane deformation models shows that for both systems a composite model consisting of molecular diffusion and continuum deformation best describes the frequency dispersion. Numerical values for the combined fit may be found in the figure legend and are similar to those reported previously [46]. In comparable studies where only continuous segmental diffusion models were invoked [138–140], faster segmental correlation times of approximately nanoseconds in the liquid-crystalline state were obtained. These fast motions contribute to the high frequency tails shown in Fig. 6. Additionally, the low-frequency contributions invoked in the fit to the composite model correlate well with the slower, three-site molecular hop correlation times (approximately microseconds) obtained by lineshape simulations for the saturated lipid DPPC [111].

Extension of the variable frequency range, from MHz down to Hz values, has shown that collective fluctuations play an important role in membrane dynamics over the entire range investigated [8,141]. This contribution is suggested by relaxation rate-frequency dispersions recorded in T_{2CPMG} experiments, where frequencies below 50 kHz are employed in the multi-pulse NMR measurements [121,142]. Additional low-frequency field-cycling techniques, where T_{1Z} measurements may be conducted at Larmor frequencies in the MHz to Hz range, have been conducted [143]. A significant ^1H NMR T_{1Z} dispersion in the range of 300 MHz down to 100 Hz allowed for the extraction of correlation times assigned to translationally-induced rotations [144] on the microsecond scale [145]. More recently, Redfield and coworkers have used a sample-shuttling fringe-field relaxation time measurement [146] of ^{31}P NMR [125] and ^{13}C NMR [124] and have detected similar microsecond correlation times that were assigned to rotational wobbling of the phospholipid assembly.

Motions contributing to the relaxation rates and frequency dispersion with correlation times that are much larger than the inverse of the Larmor frequency of measurement, $1/\tau_c \leq \omega_0$, are said to be in the long-correlation time regime. In these instances, the frequency dispersions depart from the single exponential behavior and require re-parameterization of the spectral densities of motion. It may be shown that in these cases the reduced spectral densities may be recast as power-law functions [122]. Such power-law scalings were initially proposed for liquid–crystals [147] and the relaxation-rate frequency behavior observed. Power-law scalings may take on a host of fractional power-law exponents, with physical interpretations corresponding to concentration and geometry-dependent dynamic modes within excluded volume, defect diffusion, and Ising-type relaxation pathways

Table 6
Unified power-law representation for quadrupolar (^{2}H) and dipolar (^{13}C–^{1}H) spin-lattice relaxation.[a,b]

Molecular diffusion model (non-collective)[c,d]
$R_{1Z}^{mol} \cong R_{1Z}^{fast} + \chi_\lambda^2 \tilde{U}_{mol} S_{fast}^2 (1 - S_{slow}^2) \tau_{slow}^{-1} \omega_0^{-2}$
$\tilde{U}_D^{mol} = 3\pi^2/5$
$\tilde{U}_C^{mol} = \frac{1}{10} N_H \pi^2 \left[(\gamma_H/\gamma_C - 1)^{-2} + 3 + 6(\gamma_H/\gamma_C + 1)^{-2} \right]$
Membrane deformation model (3D collective)[c,d,e]
$R_{1Z}^{col} \cong R_{1Z}^{fast} + \chi_\lambda^2 \tilde{U}_{col} C S_{fast}^2 \omega_0^{-1/2}$
$\tilde{U}_D^{col} = \frac{9}{20} \pi^2 \left(1 + 2\sqrt{2} \right)$
$\tilde{U}_C^{col} = \frac{3}{20} N_H \pi^2 \left[(\gamma_H/\gamma_C - 1)^{-1/2} + 3 + 6(\gamma_H/\gamma_C + 1)^{-1/2} \right]$

[a] Symbols: C, viscoelastic factor for 3D membrane deformation; γ_C, carbon magnetogyric ratio; γ_H, hydrogen magnetogyric ratio; R_{1Z}^{col}, nuclear Zeeman relaxation rate for collective motions; R_{1Z}^{fast}, nuclear Zeeman relaxation rate for fast segmental motions; R_{1Z}^{mol}, nuclear Zeeman relaxation rate for molecular motion; S_λ, generalized segmental order parameter; S_{slow}, order parameter for slow motion; τ_{slow}, correlation time for slow motion; $\tilde{U}_C^{col}$, carbon unification factor for collective motion; $\tilde{U}_C^{mol}$, carbon unification factor for molecular motion; $\tilde{U}_D^{col}$, deuterium unification factor for collective motion; $\tilde{U}_D^{mol}$, deuterium unification factor for molecular motion; ω_0, resonance frequency at a given magnetic field strength (ω_C = carbon frequency, ω_D = deuterium frequency); χ_λ, generalized anisotropic coupling constant. Further details may be found in Ref. [153].

[b] Relaxation rates are averaged over all bilayer orientations with respect to external magnetic field.

[c] Segmental order parameter $S_\lambda = S_{fast}\, S_{slow} = \langle P_2(\cos\beta_{PD}) \rangle$.

[d] Expressions for R_{1Z}^{fast} are given by $\frac{3}{2}\pi^2 \chi_Q^2 (1 - S_{fast}^2) \tau_{fast}$ and $N_H \pi^2 \chi_D^2 (1 - S_{fast}^2) \tau_{fast}$.

[e] Viscoelastic factor $C = k_B T \sqrt{\eta} / \pi \sqrt{2K^3}$ for 3D (nematic-like) membrane deformation model.

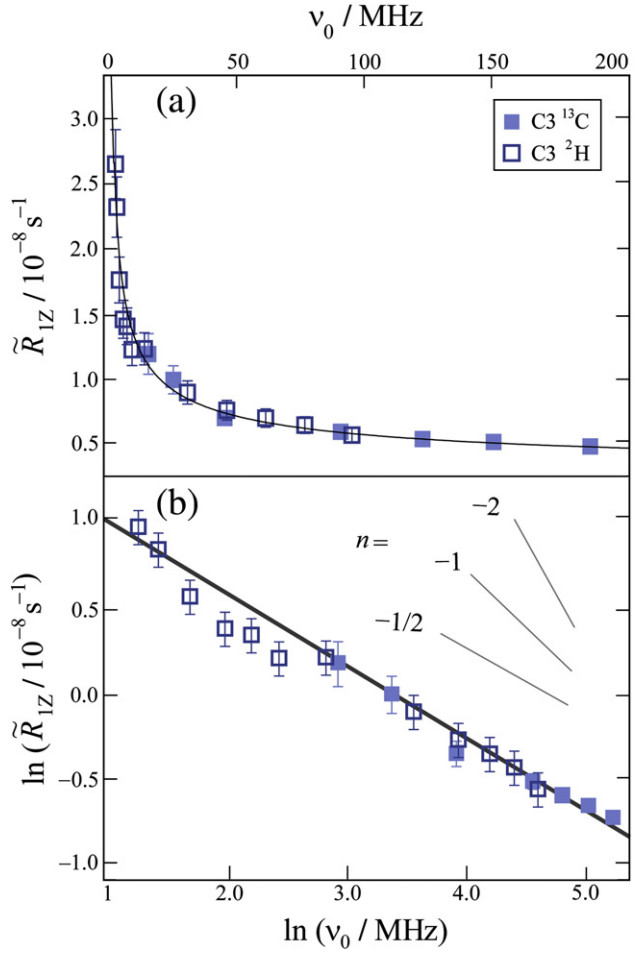

Fig. 7. Multinuclear NMR spin-lattice relaxation rates for liquid-crystalline bilayers are unified in terms of a frequency power-law. Scaled ^{2}H NMR and ^{13}C NMR spin-lattice relaxation rates $\tilde{R}_{1Z}$ may be compared simultaneously ($\nu_0 \equiv \nu_C, \nu_D$). (a) Relaxation rate dispersions for natural-abundance ^{13}C DMPC and isotopically enriched 1,2[3′, 3′-^{2}H] DMPC are shown at 30 °C. The power-law dispersions for the C3 position in (■) ^{13}C NMR and (□) ^{2}H NMR are fit by a single power-law function (—) with $n = -1/2$ consistent with a membrane deformation model. (b) Double-logarithmic plots of scaled relaxation rate dispersion with comparative fitting to alternative power-law frequency scalings as indicated. Power-law exponents are shown for $n = -2$, -1, and $-1/2$ corresponding to molecular diffusion, flexible surface (smectic deformation), and membrane deformation (nematic-like) models. Data taken in part from Refs. [46,96].

[148]. Empirical expressions involving stretched exponentials, the canonical Kohlrausch–Williams–Watts (KWW) decay, or Davidson–Cole (DC) function are commonly invoked in dielectric relaxation interpretations. These have a similar theoretical basis to NMR relaxation theories in this slow-collisional regime [149–151] such as occurs for liquid crystals and biomembranes. Similar power-law representations have been generalized, and frequency-dependent scaling of the relaxation rates have been shown to follow the relation $R_{1Z} = 1/T_{1Z} \propto \omega^{-(2-d/2)}$ [46], with the variable d describing the dimensionality of the system ($d = 1$ for one-dimensional systems such as linear polymer chains, $d = 2$ for 2D smectic bilayers, and $d = 3$ for 3D nematic systems). The power-law expressions in the long-correlation time regime derived from the spectral densities and correlation functions are shown in Table 6. In studies of organic liquid crystals utilizing CPMG measurements of the transverse relaxation rate T_2, the application of power-law expressions has shown that inverse frequency scalings are observed for pure smectic systems, and inverse square-root scalings are observed for purely nematic liquid-crystalline systems [141,152]. Using these general expressions, one may differentiate between molecular fluctuations (ns to μs) and liquid-crystalline order fluctuations (μs to ms) by the hallmark Larmor frequency dependences, as has been done in the treatment of polymeric systems [126].

One may unify the results from both ^{2}H and ^{13}C NMR experiments by scaling the rate-frequency dispersions using the results in Table 6, thus enabling the overall frequency range to be extended [153]. This is demonstrated by the scaled $\tilde{R}_{1Z}$ rates summarized in Fig. 7, where the unification of the quadrupolar and dipolar relaxation rates found in the Supplementary Content have been presented for the $(CH_2)_n$ resonance of DMPC at 30 °C. The combined dispersions represent frequency-dependent spectral density $J_m(\omega)$ contributions following a three-dimensional power-law trend ($\omega^{-1/2}$, $d = 3$) that spans nearly the full MHz regime, from 2 MHz to 938 MHz for the carbon acyl chain segments. On the other hand, a two-dimensional power law scaling (ω^{-1}, $d = 2$) of ^{31}P NMR phospholipid headgroup dynamics has been identified in T_2 measurements in the kHz regime [154,155]. The difference in the power-law scalings may reflect the sensitivity of the headgroup ^{31}P nucleus to surface or smectic-like undulations, while measurements using ^{2}H or ^{13}C as a probe of hydrocarbon dynamics may reflect the 3D anisotropy of the interior of the hydrocarbon membrane. However, despite the difference in power-law exponent, the analysis presented in these studies suggests that the non-exponential rate-frequency dispersion arises from low-frequency motion due to highly-damped order fluctuations.

It is instructive to compare the power-law dispersions of a homologous series of phospholipids to further classify the dimensionality for the motion of bilayer membranes. Using the data in Appendix A and the Supplementary Content, direct model-free comparison of differences in the relaxation rate-dispersion can be made at a set of reduced temperatures [156] relative to the gel (L_β or $L_{\beta'}$) to liquid-crystalline (L_α) transition temperature of the lipids. A power-law comparison, in a double-logarithmic presentation of the relaxation rate-dispersions for phosphatidylcholines DLPC, DMPC, and DPPC, is presented in Fig. 8 using the reduced temperatures for the homologous series with different acyl chain lengths. At approximately 10 °C above T_m for each of the lipids, the double-logarithmic dispersion exhibits a linear slope with a power-law exponent of $n = -1/2$. A simple interpretation is that the various segments of these

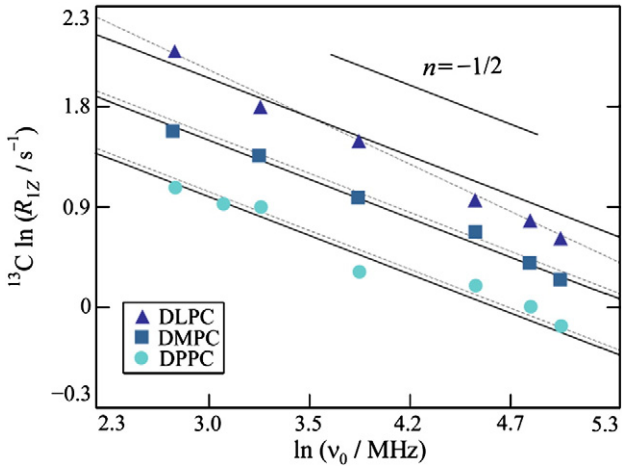

Fig. 8. Frequency power-law scaling describes non-exponential relaxation of bilayers of phosphatidylcholines over a broad temperature range in the liquid-crystalline state. Model-free analysis for natural-abundance ^{13}C NMR spin-lattice relaxation rate dispersions reveals a single power-law for a homologous series of saturated phosphatidylcholines ($\nu_0 = \nu_C$). Frequency scaling is demonstrated for the $(CH_2)_n$ carbons of (▲) DLPC at 10 °C, (■) DMPC at 30 °C, and (●) DPPC at 50 °C. Each experimental data set exhibits a best fit (– – –) close to the theoretical value of $n = -1/2$ (——) showing influence of acyl chain length on membrane dynamics. Data taken in part from Ref. [96].

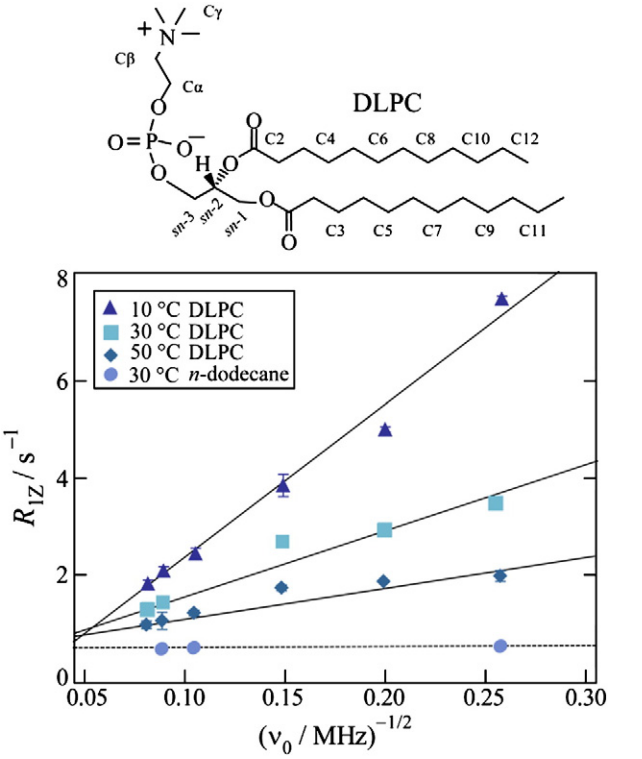

Fig. 9. Frequency dispersion of ^{13}C spin-lattice relaxation rates of liquid-crystalline DLPC membrane bilayers compared to liquid hydrocarbon. Relaxation rates obtained for the $(CH_2)_n$ segments of DLPC are shown at (▲) 10 °C, (■) 30 °C, and (♦) 50 °C. The slope of the power-law relaxation dispersion ($\nu_0 = \nu_C$) decreases with an increase in temperature versus corresponding data (●) for $(CH_2)_n$ carbons of *n*-dodecane at 30 °C. Extrapolating DPLC relaxation rates to high-frequency or high temperature approximately matches results for *n*-dodecane in the isotropic liquid state. The center of the phospholipid membrane at high temperature resembles isotropic motion of the hydrocarbon liquid. The molecular structures of *n*-dodecane and DLPC are shown. Data taken in part from Ref. [96].

saturated lipids undergo nematic-like liquid-crystalline deformations at short distances superimposed on continuous rotational diffusion, which corresponds well with the model-dependent refinement presented [157].

The NMR studies described above were foreshadowed by initial experiments which investigated pure lyotropic liquid-crystalline fatty acid systems [158], and isotropic liquid alkanes [76,159]. The basis of these observations, made by identification of the characteristic appearance of the lipid membrane in the liquid-crystalline or gel phase, was first identified in ^{1}H NMR experiments of the potassium laurate lyotropic mixture [160]. Additionally, ^{2}H quadrupolar spectra and relaxation times of perdeuterated fatty acids were recorded as a function of thermodynamic phase [158,161–165]. These studies, compared with studies of alkanes in solution, helped to establish the polarity (polar headgroup, non-polar acyl chains) of the molecule as an important factor in determining the orientational anisotropy and dynamics of the lyotropic phases. The dynamics of these systems are consistent with axially symmetric motion of the fatty acids in the liquid-crystalline state, while exotic phases such as cubic and hexagonal geometries involve changes to the orientational anisotropy and dynamics of the molecules [166]. In ^{13}C NMR, from T_{1Z} studies of a homologous series of neat alkanes it was proposed [76,77] that a two-component relaxation model involving segmental fluctuations and overall chain reorientation best represented the chain dynamics in the isotropic phase. Such observations have been important in interpreting the dynamics of the lipid acyl chains, where one end of the chain is tethered to the aqueous interface, while the terminus is free to undergo near-isotropic motion at the hydrocarbon center. However, the possibility of collective deformation modes is absent from isotropic solutions of alkanes [167,168].

A comparison of a phospholipid liquid-crystalline system to an isotropic alkane in the liquid state is illustrated in Fig. 9. Here the R_{1Z} values provided in the Supplementary Content for the $(CH_2)_n$ segments of DLPC and the liquid hydrocarbon *n*-dodecane are compared. Whereas scaling of the relaxation rates for the lipid depends on segmental motion, anisotropic molecular motion, and collective membrane motion, the relaxation rate of the alkane depends on isotropic, fast segmental and molecular motions only. The frequency dispersion for the liquid is linear with a slope nearly equal to zero at all frequencies. However for DLPC the slopes of the dispersion depend significantly on temperature. This shows that the phase behavior of the membrane contributes to the structural dynamics observed, and that the rate of the acyl chain motion becomes more like the isotropic alkane with increasing temperature, thereby highlighting the contribution of order fluctuations to the frequency dispersion. Interestingly, the ordinate intercept of the phospholipid rate dispersion in the inverse square-root presentation of the dispersion is non-zero, and is nearly the same for the $(CH_2)_n$ and liquid hydrocarbon segments. In this high-frequency limit, the relaxation rates are sensitive to the fast segmental motions and molecular reorientation of the acyl chain only. Thus, fundamentally the motions of the lipid acyl chains are similar to dynamics observed for liquid hydrocarbons, but are distinguished by molecular organization in the membrane, which allows for the possibility of lower-frequency motional contributions that arise from quasi-nematic lipid order fluctuations [8,37].

5.3. Correspondence to molecular simulations

Membrane simulations and nuclear spin relaxation studies have tended to follow a parallel course. The pioneering simulations of Richard Pastor and coworkers have demonstrated a correspondence of measured and simulated nuclear spin-lattice relaxation times [169,170]. In conjunction with experimental data provided by Brown et al. (see Supplementary Content), rotational correlation times for the lipids were calculated using closed-form analytical formalisms (cf.

Tables 4–6) [7,8,37] and were found to agree with experiment [9,78,169–171]. A current overview encompassing the current state of the art includes the membrane lipid simulations of Pastor and Feller et al. [9], as well as atomistic simulations by Edholm et al. [49], coarse-grain simulations by Marrink et al. [12,48,172], and multi-scale dynamics simulations of Ayton and Voth et al. [13,14,173]. Additionally, in the analysis of the simulations, power-law scalings resembling the $\sim\omega^{-1/2}$ frequency dependence obtained in experimental refinements were generated. Comparison of the experimental and simulation results have outlined unique properties that define the membrane dynamics. These involve molecular interactions at the aqueous interface that stabilize bilayer structure, hydrocarbon disorder in the bilayer center arising from chain torsion contributions (especially for polyunsaturated lipids), and anisotropic motion in the simulation that is necessary to reproduce the frequency dispersion trends found in experiments. One may note that these findings are correlated with the timescales of the simulation in that the contributions to the dynamics come from segmental parameterization of the bilayer force-field. These methods constrain the cross-sectional area and allow the frequency-dependent scaling of the relaxation rate to be reproduced. This has so far been representative of the all-atom strategies, which seek to reconcile discrepancies between the experimental results and simulations through modifications in the torsional potentials and finite-size boundary conditions of the simulation [99,174]. These simulation inputs represent lower limits to the scale of the force-field parameterization and the relevant contributions to the membrane dynamics considered in NMR analysis.

Bilayer order fluctuations represent the upper scale limit to the structural and dynamic regimes included in the description of the membrane [24]. The relevant measures of physical properties of the membrane at this scale involve elasticity, viscosity, and membrane curvature along with the associated bending moduli. These viscoelastic properties are fundamentally properties of the Helfrich free-energy model of the membrane [53,175]. In order to sample these motions, significant improvements in terms of the computational efficiency of the membrane simulations have been made through multi-scale simulation strategies [10–12,36,172,176]. These coarse-grained simulation approaches may rely on strictly continuum mechanics, or may incorporate aspects of quantum or molecular mechanics to steer the system [14,177]. The utility of these simulations is especially significant where the number of membrane components is exceedingly large but required in the case of lipid domains [178], and protein-containing mixed component bilayers, which undergo large-scale morphological transformations such as are involved in fusion processes [48]. Carefully designed hybrid unified-atom simulations targeting membrane properties—as in the case of the frequency-dependent relaxation rates for simple membrane systems—have detected membrane deformations that occur on a length scale larger than the molecular dimensions of the lipid. Given the proper simulation environment the emergence of slow dynamic modes is observed [10,179]. These force-fields retain a coarse-grained character resembling the atomistic simulation, while they enable the simulation to be extended to larger molecular systems and longer timescales through a reduction of the number of atoms considered in the simulation.

6. Segmental order parameters and NMR relaxation rates describe membrane structure and dynamics

6.1. Phospholipids—influences of polar headgroups and acyl chains

Nuclear magnetic resonance provides structural and dynamic information about lipid membranes whereby structure is determined from residual coupling interactions measured as anisotropic chemical shift [180–182], magnetic dipolar [66–68], and quadrupolar lineshapes [4,57,60,183–185]. For an immobilized powder, the lineshape reflects all orientations within a random distribution of phospholipids, and the full asymmetry is often required to describe the distribution, while in the hydrated liquid-crystalline phase, uniaxial rotational symmetry of the lipid about the membrane normal is evidenced by axially symmetric coupling lineshapes. The axially symmetric motions leading to dynamic averaging of the static coupling interactions may also be probed in nuclear spin relaxation measurements. In the following sections, we use the nuclear spin couplings and order parameters, together with the nuclear spin relaxation times to characterize the structure and dynamics of a variety of phospholipids with different lipid headgroups, acyl chain length and degree of unsaturation, in single-component and mixed systems.

6.1.1. Phosphatidylcholines

Saturated, unsaturated, and polyunsaturated phosphatidylcholines are well known to be vital components of cellular membranes, and comprise a major portion of the data tables in the Supplementary Content [60,186]. One significant feature of many of these lipids is that at physiological temperature the membrane remains in a fluid, liquid-crystalline (L_α) state, rather than the gel (L_β or $L_{\beta'}$) state. The influences of vinylic and allylic carbon positions on orientational order and dynamics may be probed by measurement of the segmental order parameters and relaxation times of unsaturated membrane lipid bilayers [187]. Use of separated local-field ^{13}C MAS NMR for the study of the unsaturated vinyl and allyl carbon positions has revealed that the orientational order of these central acyl positions for 1,2-dioleoyl-*sn*-glycero-3-phosphocholine (DOPC) and 1-palmitoyl-2-oleoyl-*sn*-glycero-3-phosphocholine (POPC) is significantly smaller than for the center acyl segments of saturated phosphatidylcholines [188]. The idea that the unsaturated lipid bilayer has a hydrocarbon interior that is significantly more disordered than the saturated lipid center was developed by ^{2}H NMR and X-ray experiments [92,189–191]. It was shown that the orientational order of the asymmetric lipids falls into two regions, one at the leaflet mid-plane where a universal packing curve is observed, and one at the bilayer mid-plane where terminal acyl segments of the saturated chain are more disordered as a result of the neighboring unsaturated chain [9]. This localization of flexibility offers insight into the mechanism by which nature introduces flexibility in biological membranes by alteration of the acyl packing density of the hydrocarbon core [189]. This effect has been studied extensively by ^{2}H NMR spectroscopy. Asymmetric lipids with one polyunsaturated hydrocarbon chain (*sn*-2) and one saturated chain (*sn*-1) have revealed that the unsaturation promotes localized orientational disorder in the *sn*-1 acyl chain at the region of the membrane interior where the neighboring vinyl positions are located [189,192–196]. Calculated compressibility moduli for the saturated chains in the asymmetric lipid bilayer have been found to show significant deviations from measured X-ray values [197] that reveal contributions from both saturated and unsaturated chains in chain interdigitation and packing.

The general trends observed for the rate dispersions of saturated phosphatidylcholines are also observed for the unsaturated series. Comparison of the ^{2}H spin-lattice relaxation times of the unsaturated phosphatidylcholine series with those of the saturated phosphatidylcholine lipids reveals that the relaxation rates are higher for the vinylic segments of the unsaturated acyl chains [198–200]. This is due to the larger hydrophobic volume of the vinyl segments compared to allyl or methylene sites [8,109]. Local variation of the relaxation rates at vinylic segments is also observed in unsaturated phosphatidylcholine membranes from ^{13}C NMR relaxation rate profiles [201]. This effect of unsaturation is particularly striking in the rate profile presented in Fig. 10 for 1,2-didocosahexaenoyl-*sn*-glycero-3-phosphocholine (DDPC) in the liquid-crystalline state. The plateau region of the DDPC is punctuated by high-amplitude relaxation rates for vinylic carbons, and lower relaxation rates for

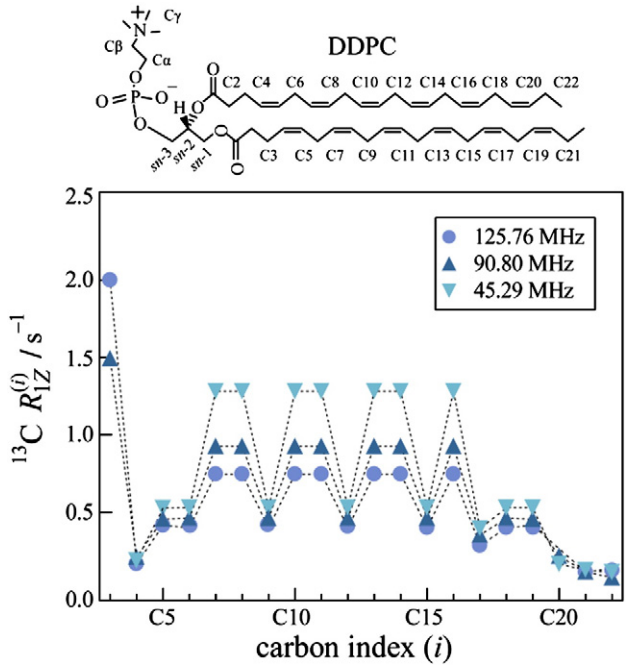

Fig. 10. Natural-abundance ^{13}C NMR spin-lattice relaxation profiles of polyunsaturated lipid bilayers show striking influences from double bonds of acyl chains. Unsaturation in the lipid membranes is observed directly for the polyunsaturated DDPC lipid. Measurements at 50 °C and Larmor frequencies ($\nu_0 = \nu_C$) of (▼) 45.29 MHz, (▲) 90.80 MHz, and (●) 125.76 MHz reveal a pronounced variation in relaxation rate. The molecular structure and assignments corresponding to the carbon index (i) are shown. Data taken in part from Ref. [201].

allylic centers. The additional allylic motion and the reduced vinylic fluctuations make the unsaturated phospholipid a versatile component of biological membranes, where both dynamic flexibility of the chains and structural rigidity of the membrane may be achieved simultaneously.

6.1.2. Phosphatidylethanolamines

The saturated phosphatidylethanolamine (PE) lipids are the second most abundant phospholipid species in biological membranes behind the phosphatidylcholines. The presence of a single amine group, rather than the trimethylammonium functional group of the PC lipids, allows for both headgroup–headgroup hydrogen bonding, and increased lipid packing efficiency [202]. This reduces the average cross-sectional area per lipid when compared to analogous saturated PCs [203]. Specific deuteration of the ethanolamine functional group has enabled solid-state ^2H NMR investigations to be performed. On the basis of ^2H NMR results in comparison with X-ray crystallographic studies, it was found that the ethanolamine headgroup extends into the aqueous partition with an orientation away from the membrane plane [204]. Following the changes of the segmental order parameter as a function of temperature for the perdeuterated *sn*-2 acyl chain of 1-myristoyl-2-perdeuteriomyristoyl-*sn*-glycero-3-phosphoethanolamine (DMPE-d_{27}) and 1,2-diperdeuteriomyristoyl-*sn*-glycero-3-phosphocholine (DMPC-d_{54}), the segmental order parameters of the PE lipids are larger than their PC counterparts, because of the decreased headgroup cross-sectional area and closer bilayer packing of the PE lipids [205].

Reduced motional degrees of freedom of the closely-packed ethanolamine lipid headgroups also contribute to the phase behavior of this lipid in pure and mixed systems, where rod-like inverse hexagonal phases, rather than planar liquid-crystalline organization may be observed at temperatures above T_m, giving rise to characteristic ^{31}P CSA lineshapes of the PE headgroup [203,206–208]. These lineshapes exhibit axial symmetry, but are scaled by $-1/2$ relative to those lineshapes measured for bilayer membranes [180,209–213], and have high-frequency $\sigma_\perp$ transitions owing to the change in chemical environment of the PE lipid headgroup in the inverted hexagonal (H_{II}) phase. This is because the symmetry axis is now along the principal (long axis) of the H_{II} cylinder, rather than along the bilayer normal of the lamellar phase. The polymorphic phase behavior of the PE system has also been studied by solid-state ^2H and ^{31}P NMR spectroscopy [214–218]. These studies focused on the thermotropic polymorphism of the PE system in the transition from the liquid-crystalline to inverted hexagonal (H_{II}) phase. The radial distribution of phospholipids about the circumference of the cylinder is in rapid exchange due to translational diffusion. In an interesting application of transverse relaxation time measurements, the circumference of the cylindrical lipid phase of 1-perdeuteriopalmitoyl-2-linoleoyl-*sn*-glycero-3-phosphoethanolamine (PLPE-d_{31}) was determined to be roughly 32 Å by comparison of the H_{II} phase relaxation times with the planar L_α relaxation times, and the dominant relaxation mechanism was proposed to be diffusion about the circumference of the H_{II} rods [203,219].

6.1.3. Phosphatidylinositols and phosphatidylserines

The headgroup of saturated and unsaturated phosphatidylinositol (PI) and phosphatidylserine (PS) membrane lipids represents a diversification of lipid structure selected by nature to fulfill a specific functional role in the cellular membrane system. From a structural and dynamic perspective, solid-state NMR studies are particularly appropriate, since specific sites of the lipid may be probed by introduction of NMR-active isotopes, or with natural-abundance ^{31}P and ^{13}C NMR spectroscopy.

For inositol polyphosphate substituents, hydrolysis of the headgroup leads to signal transduction at the endoplasmic reticulum mediated by specific binding events with charged proteins [220], and is an important component of detergent-insoluble raft domains [42]. Using ^{31}P NMR, the charged (anionic) inositol polyphosphate headgroup was shown to promote bilayer phase formation from inverted hexagonal systems of PE lipids [221]. The charge distribution of the polyphosphate headgroup is responsible for the unique inter-lipid and intra-lipid interactions of this signaling lipid. This was studied by solid-state ^{31}P MAS NMR [222] as a function of pH. Isotropic ^{31}P MAS NMR chemical shifts and static ^{31}P NMR CSA lineshapes of polyphosphate inositol were compared to reveal site-specific charge reorganization at the bilayer interface [222]. The study demonstrated that each of the monoester sites exhibit different intramolecular hydrogen bonding interactions. In conjunction with inositol ring orientation, which has been shown to extend into the aqueous layer [223], these site-specific electrostatic and dynamic variations lend the lipid properties that are important for signaling in the cellular environment [224,225].

The phosphatidylserine (PS) lipid is another charged lipid that is well studied via selective deuteration of the headgroup, glycerol backbone, and acyl chain regions, in conjunction with natural-abundance ^{31}P NMR CSA measurements. This experimental approach has revealed important similarities and differences between the PS and PC lipids [226]. One feature that sets the PS membrane apart from zwitterionic PCs is the sensitivity to the presence of monovalent and divalent cations [227–233]. Changes in lipid dynamics and membrane polymorphism are inferred from the appearance of the ^{31}P CSA and ^2H RQCs of phosphoserine headgroups. These spectral changes reflect an electrostatic stabilization of headgroup fluctuations that may occur through reduction of the lipid diffusion rate within a bilayer, or through salt-mediated inter-bilayer coupling that would change the morphology of the vesicles. The dependence of PS lipid dynamics and membrane shape on cation concentration is key in membrane fusion and interfacial binding.

6.2. Glycolipids and sphingolipids—effects on NMR observables

Additional surface modifications arise from glycosylation of the phosphate headgroup, as well as through backbone modifications. Gangliosides and cerebrosides are well studied utilizing multinuclear NMR spectroscopy, which can probe the glycosylated substrate, as well as the functionalized backbone, acyl chains, and headgroups [234–240]. As was observed in the case of glycerophospholipid (PE, PS, and PI) membranes, diversification of the type of headgroup is an important aspect for the phase behavior of a lipid membrane. Solid-state ^{2}H NMR spectra have been recorded as a function of temperature for the galactosylceramide (GalCer) sphingolipid that had been perdeuterated at the 18:0 or 24:0 chains [241–244]. The long chain lipids were postulated, on the basis of the large segmental order parameters at the terminal region of the chain, to extend across the bilayer, or fold into the bilayer mid-plane. Additionally, the miscibility of the glycosylated lipids in PC bilayers was found to be concentration dependent, with high concentrations above 20 wt.% glycosylated lipid resulting in phase separation, while at low concentrations the glycolipid and host matrix were fully miscible. Similar findings have been obtained where quadrupolar couplings and spin-lattice relaxation times have been measured for both the upper acyl C2 segmental position, glycerol backbone, and specific sites in the pyranose sugar of the glucosylceramide (GlcCer) and GalCer headgroup-modified lipids in host PC membrane bilayers [245–247]. The glycosylated headgroup was found on average to reduce the internal rotational dynamics of the lipid, measured from the segmental order parameters of the upper acyl chain, as compared with properties of similar PCs. The orientation of the glycosylated headgroup was found to be essentially normal to the bilayer plane in these cases, with a restricted orientational range established by the allowed dihedral angles of the glycerol backbone. Motionally-averaged spectral lineshapes for short chain fatty acids were well described by rapid *trans–gauche* isomerizations and rotational dynamics. Restricted rotational diffusion possibly reflects the initial formation of glycolipid-rich regions that nucleate raft formation when concentration increases [248].

7. Cholesterol and proteins affect NMR order parameters and relaxation rates of membrane lipids

7.1. Cholesterol and lipid rafts

Interactions between lipids in membranes of heterogeneous composition leads to different phase behavior, order parameters, and relaxation times versus those observed in simple lyotropics (lipid and water) [249–257]. Interest in membranes containing cholesterol (Chol) has been fostered by the idea of raft formation due to non-ideal lipid mixing [43]. The raft is a phase-separated (nano–micro) domain corresponding to cholesterol-rich liquid-ordered (l_o) and liquid-disordered (l_d) lipid phases, which are dependent upon the molar percentage of cholesterol in the membrane and temperature [258–260]. The lipid-raft is formed through an interplay of hydrocarbon mismatch, polarity of the headgroup, and the presence of additional components such as sterols or integral membrane proteins that may interact through charge pairing, hydrogen-bonding, and non-covalent van der Waals contacts [261,262]. The approach of utilizing multiple biophysical techniques—such as fluorescence spectroscopy and solid-state NMR—together has resulted in complementary measures [263] that may be confirmed in dynamics simulations [178,264].

Specific deuteration of both the saturated phosphatidylcholine lipid and cholesterol has revealed superposition ^{2}H NMR spectra indicative of phase coexistence [258,259,265–267]. The local changes to the lipid organization were also probed by selective deuteration of the C2 segmental positions of the *sn*-1 and *sn*-2 chains in experiments [80,268] that showed the RQCs of these resonances increase for DPPC/Chol mixtures below ~25 mol% cholesterol in the liquid-crystalline phase at 43 °C. Below the L_β to L_α phase transition a decreasing trend in quadrupolar splitting for the C2 resonances was observed. Similar observations were made from the perspective of the deuterated cholesterol molecule. It was demonstrated on the basis of geometrical arguments that in the liquid-disordered phase, cholesterol acts to order the neighboring lipids, while below the phase transition the liquid-ordered phase is rendered more disordered by cholesterol [269,270]. The condensed molecular headgroup geometry of the PE lipid also results in unique behavior in PE/Chol bilayers [182,271–276]. Rather than the distinct L_β to L_α phase transition observed in the PC/Chol system for the PE lipids, a continuous phase transition is observed, with the onset temperature decreasing with additional cholesterol concentration [277]. Interpretation of this observation in terms of a cooperative rapid process (μs), involving small PE/Chol domains, is in striking contrast to the more abrupt phase transition of PC/Chol mixtures. Nuclear spin-lattice relaxation and pulsed-field gradient measurements of DLPC/Chol oriented membranes have provided an additional time domain to the measurement. Reduced off-axial rotation of lipid molecules was estimated to take place at a rate 10-fold faster rate than for pure lipid membranes, owing to the ordering influence of the locked sterol ring system [278,279].

Measurement of the isotropic ^{13}C, ^{1}H, and ^{31}P NMR chemical shifts using MAS at natural isotopic abundance have identified putative regions of interaction that are characteristic of phase domains created as a function of temperature and composition [280,281]. These are suggestive of hydrophobic van der Waals interactions and intermolecular as well as intramolecular hydrogen-bonding. The local interactions between lipids that are responsible for the lateral phase immiscibility are a feature of significant interest, since it is believed that sphingomyelin–cholesterol interactions at the plasma membrane are implicated in intracellular signaling [282–284]. The rate of uptake of cholesterol into the membrane is increased by the presence of sphingomyelin, and it has been shown by isothermal titration calorimetry that the physical mechanism for this increase is expressed as a highly exothermic process that is weakly entropically favorable [285]. The origin of the thermodynamic stabilization has been shown experimentally to be due mostly to van der Waals hydrophobic interactions, as well as to hydrogen-bonding between donor and acceptor sites [286,287]. These studies have been supplemented by atomistic molecular dynamics simulations providing trajectories targeting specific interactions involving hydrogen bonding, charge pairing, and van der Waals dispersion forces between lipids, and between lipids and cholesterol in the ternary system that have confirmed the experimental interpretations [261].

The sensitivity of the order parameter to changes in hydrocarbon ordering has enabled comprehensive measures to be obtained for the domain-coexistence regimes in these systems [288]. Using ^{2}H NMR, structural and thermodynamic properties of binary and ternary systems of the canonical POPC/N-palmitoyl sphingomyelin (PSM)/Chol mixture (1:1:1) have been investigated. The presence of two-phase coexistence (l_d, l_o) in various combinations was confirmed on the basis of estimated hydrocarbon chain lengths and cross-sectional areas per lipid at selected regions of the ternary phase diagram [249]. In a comparable study, ^{2}H NMR and fluorescence microscopy provided estimates of the equilibrium domain sizes in the prototypical POPC/PSM/Chol system in the range of 45–75 nm at 40 °C [289]. In coarse-grain simulations the dimensions of the coexisting phase domains were similar, but also revealed the dynamics of the membrane with exchange of membrane components occurring on long microsecond timescales [178].

Such findings from the NMR experiments taken with other complementary experiments have shown that coexistence regimes are observed over a range of compositions and temperatures. These results have been summarized in excellent reviews [262,290] and

extensive phase diagrams have recently been compiled by Marsh [260]. The characterization of domain formation and boundaries of phase coexistence has been furthered by recent X-ray investigations conducted on ternary systems that have made use of synchrotron beam sources [291,292]. The high-resolution results from these experiments have confirmed the presence of fluid and cholesterol-enriched ordered phases in the two-phase coexistence regions of membrane composition within the complex diagrams [260].

7.2. Membrane lipid–protein interactions

The phospholipid membrane has a multifunctional role that depends on the properties of the lipids. In some instances, the membrane acts as a passive structure for peripheral protein–membrane interactions [293,294]; in others the membrane serves as a host for the alignment and activation of transmembrane proteins [295–297]. In these cases, deformation or dissolution similar to that observed in model lipid-surfactant systems [298–306] occurs in the presence of anti-microbial and pore-forming species [307–309]. The membrane may also be remodeled in the presence of curvature-sensing membrane fusion proteins [42,310]. On the other hand, the membrane itself can be viewed as causing the activation of peripheral and transmembrane proteins. This may occur via a surface-mediated conformational stabilization, as in the folding of intrinsically disordered proteins such as α-synuclein [311,312], or the membrane tension sensing of transmembrane mechanosensitive proteins [313]. These membrane properties may be investigated by using NMR and molecular dynamics studies where segmental order and relaxation times are obtained. The results of such novel experiments may be interpreted through comparison with the benchmark studies and measurements discussed in this review.

Lastly, interaction of the proteins with their natural membrane bilayer has been extensively studied for both natural protein-containing membranes and reconstituted systems [314,315]. Measurements obtained in these structural and dynamics studies may be found in the Supplementary Content. High-resolution ^{1}H NMR and ^{13}C NMR studies of rod outer segment membranes, containing the G protein-coupled receptor rhodopsin, have characterized the highly polyunsaturated lipids making up the membrane [316–322]. This presence of a large proportion of polyunsaturated PE lipids has been shown to be coupled with the photoactivation of rhodopsin [41,323]. For extracted lipids and the intact rod outer segment membranes, ^{31}P NMR measurements of the residual CSA suggest that the headgroup orientation of the PC and PE lipids is not significantly changed by the presence of this protein. Similar findings were reported for the sarcoplasmic reticulum lipid Ca^{2+}-ATPase membrane system [324–326]. Acyl chain ordering as measured from ^{2}H NMR lineshapes was shown to be nominally sensitive to the reconstitution of rhodopsin in deuterated lipids [35,327–329]. However, it was later shown that while the quadrupolar splittings of the ^{2}H acyl chain segments do not change appreciably in the presence of the protein, the overall phase behavior as determined from temperature-dependent relaxation time measurements of the proteolipid system do show drastic differences versus pure membrane lipid control systems. Analogous conclusions have been reached by Akutsu and coworkers in reconstitution experiments of the subunit *c*-ring of the ATP synthase motor protein in DMPC bilayers [330]. These observations suggest that the lipids and proteins may be intrinsically coupled, not through local segmental perturbation where large excursions of segmental orientations would be observed through striking changes of order parameters, but rather through the viscoelastic continuum properties of the membrane as detected in the relaxation time measurements. Here mesoscale properties such as curvature and order-director fluctuations of the membrane may be envisioned to effect the formation of an ion-passing pore, or fusion of neighboring bilayers through peptide-induced changes of bilayer curvature.

8. Future insights are possible by combining molecular simulations with NMR spectroscopy

From the benchmark studies presented here, there is a clear trend in membrane research towards multi-component systems consisting of multiple lipid types, various sterols, and a host of proteins. The importance of these systems springs from a paradigm whereby the structure and dynamics are intrinsically coupled with membrane function [43,331] as facilitated by the benchmark studies highlighted in this review. NMR studies have demonstrated that the liquid-crystalline properties of the phospholipid bilayers give rise to characteristic experimental observables that are explainable by atomistic and continuum models. From an atomistic perspective, the structure and dynamics observed in large part are determined by the properties of the lipid, depending on the number of carbons in the acyl chain, headgroup type, and degree of unsaturation. Additionally, membrane structural dynamics are influenced by the presence of components such as water, cholesterol, peptides, and proteins. Along with this atomistic picture of the membrane, collective or continuum models exist that describe the membrane as a viscoelastic mesoscopic material. In this representation, thermodynamic ensembles of lipids and membrane components contribute to the dynamic structure of the membrane. This is a universal feature of the dynamics observed for the phosphatidylcholine membrane systems studied in the NMR experiments. As studies of membranes proceed towards ever more complex systems, NMR becomes faster and more sensitive, and dynamics simulations evolve for longer trajectories, the fundamental measures and interpretations become more valuable. The synergy of structural and dynamics measurements presented and interpreted using analytical models, and with simple heuristic examples in this contribution, will crystallize these benchmark results for those beginning and continuing research in the field.

Acknowledgements

We thank T. Allen, O. Edholm, S. Feller, R. Pastor, H. Petrache, A. Redfield, K. Schulten, A. Szabo, G. Voth, and members of the laboratory for discussions. Database entries may be found at http://cbc.arizona.edu/brown/group/database. Financial support from the U.S. National Institutes of Health is gratefully acknowledged.

Appendix A

The experimental NMR database is found in the Supplementary Content and on the Brown Laboratory website (http://cbc.arizona.edu/brown/group/database). The database contains ^{2}H and ^{13}C segmental order parameters (S_{CD}, S_{CH}), nuclear Zeeman spin-lattice relaxation times (T_{1Z}), and details of the NMR measurements. Order parameters and relaxation times for membrane lipids and related systems are organized in terms of acyl chain length, degree of unsaturation, headgroup type, and sample composition at multiple temperatures and different Larmor frequencies (magnetic field strengths). Solid-state ^{2}H NMR data are included for multilamellar lipid dispersions. Complementary ^{13}C NMR data refer to unilamellar vesicle suspensions studied with solution NMR techniques and multilamellar dispersions investigated with solid-state NMR. The Appendix provides a representative example for DMPC in the liquid-crystalline (L_α or l_d) state as a guide to the additional data that are provided online.

Table A1
^{2}H NMR segmental order parameters (S_{CD}) and spin-lattice relaxation times (T_{1Z} / ms) of DMPC-d_{54} [a,b].

T / °C	ν_0 / MHz		C2[c]	C3	C4	C5	C6	C7	C8	C9	C10	C11	C12	C13	C14
30	46.10	S_{CD}[d]	0.212	0.212	0.212	0.212	0.212	0.212	0.202	0.193	0.175	0.121	0.105	0.090	0.026
			(0.121/0.090)	(0.212)	(0.212)	(0.212)	(0.212)	(0.212)	(0.202)	(0.202)	(0.193)	(0.175)	(0.121)	(0.090)	(0.026)
		T_{1Z}	26.8	26.8	26.8	26.8	26.8	26.8	29.1	31.7	41.8	79.8	108	111	319
			±0.3	±0.3	±0.3	±0.3	±0.3	±0.3	±1.1	±1.2	±1.1	±1.6	±2.3	±1.8	±1.6
			(79.8 / 111)	(26.8)	(26.8)	(26.8)	(26.8)	(26.8)	(29.1)	(29.1)	(31.7)	(41.8)	(79.8)	(111)	(319)
			(±1.6/ ±1.0)	(±0.3)	(±0.3)	(±0.3)	(±0.3)	(±0.3)	(±1.1)	(±1.1)	(±1.2)	(±1.1)	(±1.6)	(±1.8)	(±1.6)
	55.43	S_{CD}[d]	0.209	0.209	0.209	0.209	0.209	0.209	0.199	0.181	0.170	0.147	0.125	0.099	0.026
			(0.147 / 0.099)	(0.209)	(0.209)	(0.209)	(0.209)	(0.209)	(0.199)	(0.181)	(0.170)	(0.147)	(0.125)	(0.099)	(0.026)
		T_{1Z}	25.4	25.4	25.4	25.4	25.4	25.4	27.8	34.8	42.3	44.8	62.6	70.5	298
			±0.8	±0.8	±0.8	±0.8	±0.8	±0.8	±0.9	±2.0	±4.0	±5.1	±6.5	±9.0	±8.1
			(44.8 / 70.5)	(25.4)	(25.4)	(25.4)	(25.4)	(25.4)	(27.8)	(34.8)	(42.3)	(44.8)	(62.6)	(70.5)	(298)
			(±5.1 /±9.0)	(±0.8)	(±0.8)	(±0.8)	(±0.8)	(±0.8)	(±0.9)	(±2.0)	(±4.0)	(±5.1)	(±6.5)	(±9.0)	(±8.1)
	76.78	S_{CD}[d]	0.226	0.226	0.226	0.226	0.226	0.226	0.202	0.184	0.169	0.148	0.125	0.092	0.027
			(0.148 / 0.092)	(0.226)	(0.226)	(0.226)	(0.226)	(0.226)	(0.202)	(0.184)	(0.169)	(0.169)	(0.139)	(0.111)	(0.027)
		T_{1Z}	34.1	34.1	34.1	34.1	34.1	34.1	46.4	46.4	53.0	50.6	78.8	103	326
			±0.5	±0.5	±0.5	±0.5	±0.5	±0.5	±1.0	±1.0	±15.4	±2.1	±1.9	±5.2	±16.3
			(50.6 / 103)	(34.1)	(34.1)	(34.1)	(34.1)	(34.1)	(46.4)	(46.4)	(53.0)	(53.0)	(67.3)	(104)	(326)
			(±2.1 / ±5.2)	(±0.5)	(±0.5)	(±0.5)	(±0.5)	(±0.5)	(±1.0)	(±1.0)	(±15.4)	(±15.4)	(±2.2)	(±3.4)	(±16.3)
	115.10	S_{CD}[d]	0.218	0.218	0.218	0.218	0.218	0.218	0.210	0.203	0.142	0.129	0.114	0.095	0.027
			(0.129 / 0.095)	(0.218)	(0.218)	(0.210)	(0.203)	(0.186)	(0.172)	(0.151)	(0.142)	(0.129)	(0.114)	(0.095)	(0.027)
		T_{1Z}	37.2	37.2	37.2	37.2	37.2	37.2	41.4	46.1	69.4	87.8	114	98.0	314
			±0.4	±0.4	±0.4	±0.4	±0.4	±0.4	±0.4	±0.5	±0.7	±0.9	±1.1	±1.0	±3.1
			(87.8 / 98.0)	(37.2)	(37.2)	(37.2)	(37.2)	(37.2)	(63.0)	(63.4)	(69.4)	(87.8)	(114)	(98.0)	(314)
			(±0.9 / ±1.0)	(±0.4)	(±0.4)	(±0.4)	(±0.4)	(±0.4)	(±0.6)	(±0.6)	(±0.7)	(±0.9)	(±1.1)	(±1.0)	(±3.1)
50	46.10	S_{CD}[d]	0.182	0.182	0.182	0.182	0.182	0.167	0.154	0.142	0.125	0.108	0.092	0.067	0.019
			(0.108/ 0.067)	(0.182)	(0.182)	(0.182)	(0.182)	(0.167)	(0.167)	(0.154)	(0.142)	(0.125)	(0.108)	(0.077)	(0.019)
		T_{1Z}	40.0	40.0	40.0	40.0	40.0	44.6	52.4	68.3	70.0	115	158	207	467
			±0.5	±0.5	±0.5	±0.5	±0.5	±1.8	±2.1	±4.3	±1.9	±7.9	±10.7	±13.9	±9.8
			(115 / 207)	(40.0)	(40.0)	(40.0)	(40.0)	(44.6)	(44.6)	(52.4)	(68.3)	(70.0)	(115)	(207)	(467)
			(±7.9 / ±13.9)	(±0.5)	(±0.5)	(±0.5)	(±0.5)	(±1.8)	(±1.8)	(±2.1)	(±4.3)	(±1.9)	(±7.9)	(±13.9)	(±9.80)
	55.43	S_{CD}[d]	0.168	0.168	0.168	0.168	0.168	0.159	0.159	0.141	0.127	0.113	0.094	0.070	0.020
			(0.113 / 0.094)	(0.168)	(0.168)	(0.168)	(0.168)	(0.159)	(0.168)	(0.159)	(0.141)	(0.127)	(0.104)	(0.082)	(0.020)
		T_{1Z}	38.4	38.4	38.4	38.4	38.4	44.0	44.0	56.4	57.1	70.0	82.1	143	430
			±1.9	±1.9	±1.9	±1.9	±1.9	±2.2	±2.2	±3.8	±3.3	±6.8	±6.7	±14.5	±16.8
			(70.0 / 82.1)	(38.4)	(38.4)	(38.4)	(38.4)	(44.0)	(38.4)	(44.0)	(56.4)	(57.1)	(91.3)	(127)	(430)
			(±6.8 / ±6.7)	(±1.9)	(±1.9)	(±1.9)	(±1.9)	(±2.2)	(±1.9)	(±2.2)	(±3.8)	(±3.3)	(±9.0)	(±8.9)	(±16.8)
	76.78	S_{CD}[d]	0.187	0.187	0.187	0.176	0.165	0.155	0.138	0.128	0.110	0.100	0.079	0.079	0.019
			(0.100/0.079)	(0.187)	(0.187)	(0.176)	(0.165)	(0.155)	(0.138)	(0.128)	(0.110)	(0.110)	(0.100)	(0.079)	(0.019)
		T_{1Z}	38.9	38.9	38.9	38.9	38.9	46.7	44.0	58.7	59.5	82.5	80.5	107	369
			±0.9	±0.9	±0.9	±0.9	±0.9	±4.1	±2.7	±2.4	±3.0	±6.6	±5.6	±4.3	±18.9
			(82.5 / 107)	(38.9)	(38.9)	(38.9)	(38.9)	(46.7)	(46.7)	(44.0)	(58.7)	(59.5)	(80.5)	(106)	(369)
			(±6.6 / ±4.3)	(±0.9)	(±0.9)	(±0.9)	(±0.9)	(±4.1)	(±4.1)	(±2.7)	(±2.4)	(±3.0)	(±5.6)	(±5.2)	(±18.9)
65	46.10	S_{CD}[d]	0.172	0.172	0.172	0.161	0.161	0.149	0.149	0.117	0.099	0.090	0.082	0.060	0.016
			(0.090 / 0.060)	(0.172)	(0.172)	(0.161)	(0.161)	(0.149)	(0.149)	(0.131)	(0.117)	(0.099)	(0.090)	(0.071)	(0.016)
		T_{1Z}	61.3	61.3	61.3	58.3	58.3	66.7	66.7	119	139	210	239	381	793
			±1.5	±1.5	±1.5	±1.2	±1.2	±1.6	±1.6	±3.6	±7.9	±7.1	±13.7	±89.1	±12.5
			(210 / 381)	(61.3)	(61.3)	(58.3)	(58.3)	(66.7)	(66.7)	(96.8)	(119)	(139)	(210)	(324)	(793)
			(±7.1 / ±8.9)	(±1.5)	(±1.5)	(±1.2)	(±1.2)	(±1.6)	(±1.6)	(±3.3)	(±3.6)	(±7.9)	(±7.1)	(±33.3)	(±12.5)
	55.43	S_{CD}[d]	0.170	0.170	0.170	0.163	0.163	0.149	0.138	0.121	0.110	0.094	0.080	0.059	0.015
			(0.121 / 0.094)	(0.170)	(0.170)	(0.163)	(0.163)	(0.149)	(0.138)	(0.138)	(0.121)	(0.110)	(0.087)	(0.068)	(0.015)
		T_{1Z}	43.3	43.3	43.3	46.6	46.6	51.4	57.4	63.7	79.3	85.1	136	180	573
			±2.2	±2.2	±2.2	±2.0	±2.0	±3.6	±3.8	±4.5	±7.0	±10.2	±17.5	±35.6	±14.6
			(63.7 / 85.1)	(43.3)	(43.3)	(46.6)	(46.6)	(51.4)	(57.4)	(57.4)	(63.7)	(79.3)	(108)	(182)	(573)
			(±4.5 / ±10.2)	(±2.2)	(±2.2)	(±2.0)	(±2.0)	(±3.6)	(±3.8)	(±3.8)	(±4.5)	(±7.0)	(±8.7)	(±24.9)	(±14.6)
	76.78	S_{CD}[d]	0.170	0.170	0.170	0.155	0.155	0.144	0.125	0.112	0.097	0.089	0.081	0.069	0.016
			(0.112 / 0.089)	(0.170)	(0.170)	(0.155)	(0.155)	(0.144)	(0.125)	(0.125)	(0.112)	(0.097)	(0.089)	(0.060)	(0.016)
		T_{1Z}	56.7	56.7	56.7	60.8	60.8	68.5	80.3	119	95.6	187	196	290	833
			±1.6	±1.6	±1.6	±2.0	±2.0	±2.9	±3.8	±9.4	±6.4	±19.1	±13.4	±28.3	±161.0
			(119 / 187)	(56.7)	(56.7)	(60.8)	(60.8)	(68.5)	(80.3)	(80.3)	(119.0)	(95.6)	(187)	(302)	(833)
			(±9.4 / ±6.4)	(±1.6)	(±1.6)	(±2.0)	(±2.0)	(±2.9)	(±3.8)	(±3.8)	(±9.4)	(±6.4)	(±19.1)	(±34.5)	(±161.0)

[a] DMPC-d_{54} is an abbreviation for 1,2-diperdeuteriomyristoyl-*sn*-glycero-3-phosphocholine. Data are for multilamellar dispersions at pH≈7 (typically in 0.1 M phosphate buffer). Values for the *sn*-1 chains are given first followed by the values for *sn*-2 chains in parentheses.
[b] Data are taken in part from Ref. [95].
[c] For the C2 segment of the *sn*-2 acyl chain values for the two nonequivalent deuterons are indicated separately (*sn*-2*a* / *sn*-2*b*).
[d] Absolute value; for sign of S_{CD} see Ref. [60].

Table A2
^{13}C NMR segmental order parameters (S_{CH}) and spin-lattice relaxation times (T_{1Z} / s) for DMPC[a,b].

T / °C	ν_0 / MHz		Cα	Cβ	Cγ	*sn*-1	*sn*-2	*sn*-3	C2	C3	C4-C8	C9-C11	C12	C13	C14
30	125.76	S_{CH}[d,e]	0.034	0.034	0.017	0.231	0.207	0.018	0.120	0.207	0.195	0.169	0.126	0.091	0.018
	15.04[c]	T_{1Z}	0.164	0.134	0.372	0.061	–	0.161	0.179	0.177	0.242	0.242	0.379	0.694	2.065
			±0.018	±0.017	±0.008	±0.024	–	±0.024	±0.026	±0.017	±0.006	±0.006	±0.030	±0.057	±0.082
	25.15[c]	T_{1Z}	0.170	0.176	0.387	–	–	0.099	0.202	0.243	0.294	0.294	0.462	0.811	1.946
			±0.026	±0.021	±0.051	–	–	±0.027	±0.027	±0.060	±0.016	±0.016	±0.042	±0.117	±0.219
	45.29[c]	T_{1Z}	0.263	0.279	0.419	0.099	0.170	–	0.243	0.296	0.408	0.408	0.582	1.265	2.570
			±0.038	±0.046	±0.011	±0.027	±0.061	–	±0.025	±0.034	±0.015	±0.015	±0.056	±0.119	±0.120
	90.80[c]	T_{1Z}	0.285	0.320	0.406	0.139	0.198	0.186	0.326	0.388	0.523	0.523	0.912	1.530	2.600
			±0.025	±0.030	±0.007	±0.014	±0.051	±0.070	±0.024	±0.060	±0.027	±0.027	±0.041	±0.103	±0.143
	125.76[c]	T_{1Z}	0.383	0.384	0.533	0.149	0.179	0.149	0.350	0.337	0.664	0.664	1.058	1.734	3.036
			±0.030	±0.025	±0.013	±0.036	±0.035	±0.036	±0.014	±0.025	±0.005	±0.005	±0.055	±0.086	±0.099
	125.76[d]	T_{1Z}	0.280	0.285	0.369	0.222	0.262	0.222	0.325	0.223	0.556	0.556	1.009	1.264	2.293
			±0.020	±0.022	±0.024	±0.031	±0.051	±0.031	±0.022	±0.138	±0.040	±0.040	±0.180	±0.007	±0.148
	150.84[c]	T_{1Z}	0.370	0.353	0.479	0.199	0.246	0.199	0.448	0.512	0.745	0.745	1.962	2.483	4.209
			±0.021	±0.039	±0.022	±0.018	±0.041	±0.018	±0.046	±0.036	±0.095	±0.095	±0.250	±0.236	±0.568
	188.70[c]	T_{1Z}	–	–	–	–	–	–	–	0.632	0.828	0.828	–	–	–
			–	–	–	–	–	–	–	±0.038	±0.016	±0.016	–	–	–
50	125.76	S_{CH}[d,e]	0.034	0.030	0.018	0.221	0.191	0.018	0.112	0.178	0.160	0.125	0.094	0.065	0.018
	15.04[c]	T_{1Z}	0.322	0.351	0.763	0.069	0.097	0.069	0.234	0.305	0.456	0.456	0.788	1.652	3.645
			±0.056	±0.062	±0.025	±0.012	±0.034	±0.012	±0.029	±0.042	±0.014	±0.014	±0.050	±0.154	±0.124
	25.15[c]	T_{1Z}	0.291	0.407	0.737	0.064	–	0.082	0.279	0.364	0.488	0.488	0.899	1.607	3.485
			±0.030	±0.047	±0.045	±0.010	–	±0.013	±0.068	±0.040	±0.024	±0.024	±0.130	±0.135	±0.291
	45.29[c]	T_{1Z}	0.383	0.490	0.798	0.109	0.175	0.111	0.287	0.516	0.568	0.644	1.205	2.125	4.180
			±0.052	±0.041	±0.022	±0.016	±0.040	±0.081	±0.023	±0.047	±0.017	±0.033	±0.064	±0.131	±0.241
	90.80[c]	T_{1Z}	0.551	0.568	0.913	0.146	0.252	0.215	0.410	0.608	0.776	0.846	1.685	2.445	4.030
			±0.048	±0.049	±0.041	±0.020	±0.033	±0.038	±0.021	±0.037	±0.030	±0.048	±0.112	±0.099	±0.239
	125.76[c]	T_{1Z}	0.526	0.554	0.801	0.125	0.243	0.125	0.344	0.540	0.843	0.843	2.064	2.129	4.673
			±0.031	±0.027	±0.026	±0.024	±0.037	±0.024	±0.021	±0.019	±0.010	±0.010	±0.138	±0.094	±0.184
	125.76[d]	T_{1Z}	0.515	0.505	0.793	0.154	0.272	0.154	0.365	0.607	0.849	0.849	1.998	2.318	4.584
			±0.063	±0.094	±0.038	±0.063	±0.065	±0.063	±0.053	±0.084	±0.038	±0.038	±0.352	±0.326	±0.127
	150.84[c]	T_{1Z}	0.858	0.858	0.880	0.260	0.309	0.260	0.568	0.722	1.004	1.004	2.090	2.710	4.928
			±0.164	±0.164	±0.035	±0.018	±0.033	±0.018	±0.038	±0.065	±0.041	±0.041	±0.181	±0.124	±0.669
	188.70[c]	T_{1Z}	–	–	–	–	–	–	–	0.745	1.07	1.07	–	–	–
			–	–	–	–	–	–	–	±0.032	±0.01	±0.01	–	–	–

[a] DMPC is an abbreviation for 1,2-dimyristoyl-*sn*-glycero-3-phosphocholine. Data are for sonicated vesicles or multilamellar dispersions at pH≈7 (typically in 0.1 M phosphate buffer).
[b] Data are taken in part from Ref. [96].
[c] Sonicated vesicles.
[d] Multilamellar dispersions.
[e] Absolute value; for sign of S_{CH} see Ref. [67].

Appendix B. Supplementary data

Supplementary data to this article can be found online at doi:10.1016/j.bbamem.2010.11.027.

References

[1] J. Seelig, Deuterium magnetic resonance: theory and application to lipid membranes, Q. Rev. Biophys. 10 (1977) 353–418.
[2] R.G. Griffin, Solid state nuclear magnetic resonance of lipid bilayers, Meth. Enzymol. 72 (1981) 108–174.
[3] J.H. Davis, The description of membrane lipid conformation, order and dynamics by ^{2}H-NMR, Biochim. Biophys. Acta 737 (1983) 117–171.
[4] M. Bloom, E. Evans, O.G. Mouritsen, Physical properties of the fluid lipid-bilayer component of cell membranes: a perspective, Q. Rev. Biophys. 24 (1991) 293–397.
[5] M.F. Brown, Membrane structure and dynamics studied with NMR spectroscopy, in: K. Merz Jr., B. Roux (Eds.), Biological Membranes. A Molecular Perspective from Computation and Experiment, Birkhäuser, Basel, 1996, pp. 175–252.
[6] D.A. Torchia, A. Szabo, Spin-lattice relaxation in solids, J. Magn. Reson. 49 (1982) 107–121.
[7] G. Lipari, A. Szabo, Model-free approach to the interpretation of nuclear magnetic resonance relaxation in macromolecules. 1. Theory and Range of Validity, J. Am. Chem. Soc. 104 (1982) 4546–4559.
[8] M.F. Brown, Theory of spin-lattice relaxation in lipid bilayers and biological membranes. ^{2}H and ^{14}N quadrupolar relaxation, J. Chem. Phys. 77 (1982) 1576–1599.
[9] R.W. Pastor, R.M. Venable, S.E. Feller, Lipid bilayers, NMR relaxation, and computer simulations, Acc. Chem. Res. 35 (2002) 438–446.
[10] E. Lindahl, O. Edholm, Mesoscopic undulations and thickness fluctuations in lipid bilayers from molecular dynamics simulations, Biophys. J. 79 (2000) 426–433.
[11] E. Lindahl, O. Edholm, Molecular dynamics simulation of NMR relaxation rates and slow dynamics in lipid bilayers, J. Chem. Phys. 115 (2001) 4938–4950.
[12] S.J. Marrink, A.H. de Vries, A.E. Mark, Coarse grained model for semiquantitative lipid simulations, J. Phys. Chem. B 108 (2004) 750–760.
[13] G.S. Ayton, W.G. Noid, G.A. Voth, Multiscale modeling of biomolecular systems: in serial and in parallel, Curr. Opin. Struct. Biol. 17 (2007) 192–198.
[14] G.S. Ayton, S. Izvekov, W.G. Noid, G.A. Voth, Multiscale simulation of membranes and membrane proteins: connecting molecular interactions to mesoscopic behavior, Curr. Top. Membr. 60 (2008) 181–225.
[15] E.A. Golovina, A.V. Golovin, F.A. Hoekstra, R. Faller, Water replacement hypothesis in atomic detail—factors determining the structure of dehydrated bilayer stacks, Biophys. J. 97 (2009) 490–499.
[16] I. Vorobyov, B. Bekker, T.W. Allen, Electrostatics of deformable lipid membranes, Biophys. J. 98 (2010) 2904–2913.
[17] J.F. Nagle, R.T. Zhang, S. Tristram-Nagle, W.J. Sun, H.I. Petrache, R.M. Suter, X-ray structure determination of fully hydrated L_α phase dipalmitoylphosphatidylcholine bilayers, Biophys. J. 70 (1996) 1419–1431.
[18] S. Tristram-Nagle, H.I. Petrache, J.F. Nagle, Structure and interactions of fully hydrated dioleoylphosphatidylcholine bilayers, Biophys. J. 75 (1998) 917–925.
[19] H.I. Petrache, N. Gouliaev, S. Tristram-Nagle, R.T. Zhang, R.M. Suter, J.F. Nagle, Interbilayer interactions from high-resolution X-ray scattering, Phys. Rev. E 57 (1998) 7014–7024.
[20] J.F. Nagle, S. Tristram-Nagle, Structure of lipid bilayers, Biochim. Biophys. Acta 1469 (2000) 159–195.
[21] S.H. White, G.I. King, J.E. Cain, Location of hexane in lipid bilayers determined by neutron diffraction, Nature 290 (1981) 161–163.
[22] S. König, W. Pfeiffer, T. Bayerl, D. Richter, E. Sackmann, Molecular dynamics of lipid bilayers studied by incoherent quasi-elastic neutron scattering, J. Phys. II 2 (1992) 1589–1615.
[23] S.H. White, M.C. Wiener, The liquid-crystallographic structure of fluid lipid bilayer membranes, in: K. Merz Jr., B. Roux (Eds.), Biological Membranes. A Molecular Perspective from Computation and Experiment, Birkhäuser, Basel, 1996, pp. 127–144.
[24] T.M. Bayerl, Collective membrane motions, Curr. Opin. Colloid Interface Sci. 5 (2000) 232–236.
[25] E. Endress, H. Heller, H. Casalta, M.F. Brown, T. Bayerl, Anisotropic motion and molecular dynamics of cholesterol, lanosterol, and ergosterol in lecithin bilayers studied by quasielastic neutron scattering, Biochemistry 41 (2002) 13078–13086.

[26] G. Pabst, N. Kučerka, M.-P. Nieh, M.C. Rheinstädter, J. Katsaras, Applications of neutron and X-ray scattering to the study of biologically relevant model membranes, Chem. Phys. Lipids 163 (2010) 460–479.
[27] A. Holmgren, L.B.-Å. Johansson, G. Lindblom, An FT IR linear dichroism study of lipid membranes, J. Phys. Chem. 91 (1987) 5298–5301.
[28] R. Mendelsohn, M.A. Davies, J.W. Brauner, H.F. Schuster, R.A. Dluhy, Quantitative determination of conformational disorder in the acyl chains of phospholipid bilayers by infrared spectroscopy, Biochemistry 28 (1989) 8934–8939.
[29] R. Mendelsohn, Infrared spectroscopic determination of conformational disorder and microphase separation in phospholipid acyl chains, in: K. Merz Jr., B. Roux (Eds.), Biological Membranes. A Molecular Perspective from Computation and Experiment, Birkhäuser, Basel, 1996, pp. 145–173.
[30] D.F.H. Wallach, S.P. Verma, J. Fookson, Application of laser Raman and infrared spectroscopy to the analysis of membrane structure, Biochim. Biophys. Acta 559 (1979) 153–208.
[31] B.J. Litman, E.N. Lewis, I.W. Levin, Raman spectroscopic studies of multi-lamellar phosphatidylcholine dispersions, Biochemistry 30 (1991) 313–319.
[32] C. Lee, C.D. Bain, Raman spectra of planar supported lipid bilayers, Biochim. Biophys. Acta 1711 (2005) 59–71.
[33] J.F. Nagle, S. Tristram-Nagle, Lipid bilayer structure, Curr. Opin. Struct. Biol. 10 (2000) 474–480.
[34] J. Zimmerberg, K. Gawrisch, The physical chemistry of biological membranes, Nat. Chem. Biol. 2 (2006) 564–567.
[35] M.F. Brown, Modulation of rhodopsin function by properties of the membrane bilayer, Chem. Phys. Lipids 73 (1994) 159–180.
[36] F.L.H. Brown, Elastic modeling of biomembranes and lipid bilayers, Annu. Rev. Phys. Chem. 59 (2008) 685–712.
[37] M.F. Brown, Theory of spin-lattice relaxation in lipid bilayers and biological membranes. Dipolar relaxation, J. Chem. Phys. 80 (1984) 2808–2831.
[38] C. Mayer, K. Müller, K. Weisz, G. Kothe, Deuteron NMR relaxation studies of phospholipid membranes, Liq. Cryst. 3 (1988) 797–806.
[39] R. Kimmich, NMR: Tomography, Diffusometry, Relaxometry, Springer, 2001.
[40] N.J. Gibson, M.F. Brown, Lipid headgroup and acyl chain composition modulate the MI–MII equilibrium of rhodopsin in recombinant membranes, Biochemistry 32 (1993) 2438–2454.
[41] A.V. Botelho, T. Huber, T.P. Sakmar, M.F. Brown, Curvature and hydrophobic forces drive oligomerization and modulate activity of rhodopsin in membranes, Biophys. J. 91 (2006) 4464–4477.
[42] J. Rohrbough, K. Broadie, Lipid regulation of the synaptic vesicle cycle, Nat. Rev. Neurosci. 6 (2005) 139–150.
[43] R. Phillips, T. Ursell, P. Wiggins, P. Sens, Emerging roles for lipids in shaping membrane–protein function, Nature 459 (2009) 379–385.
[44] L.V. Chernomordik, M.M. Kozlov, Mechanics of membrane fusion, Nat. Struct. Mol. Biol. 7 (2008) 675–683.
[45] S.M. Gruner, Stability of lyotropic phases with curved interfaces, J. Phys. Chem. 93 (1989) 7562–7570.
[46] A.A. Nevzorov, M.F. Brown, Dynamics of lipid bilayers from comparative analysis of ^{2}H and ^{13}C nuclear magnetic resonance relaxation data as a function of frequency and temperature, J. Chem. Phys. 107 (1997) 10288–10310.
[47] H.I. Petrache, S.W. Dodd, M.F. Brown, Area per lipid and acyl length distributions in fluid phosphatidylcholines determined by ^{2}H NMR spectrscopy, Biophys. J. 79 (2000) 3172–3192.
[48] S.J. Marrink, A.H. De Vries, D.P. Tieleman, Lipids on the move: simulations of membrane pores, domains, stalks and curves, Biochim. Biophys. Acta 1788 (2009) 149–168.
[49] O. Edholm, Time and length scales in lipid bilayer simulations, Curr. Top. Membr. 60 (2008) 91–107.
[50] V. Luzzati, F. Husson, The structure of the liquid crystalline phase of lipid–water systems, J. Cell Biol. 12 (1962) 207–219.
[51] J. Charvolin, A. Tardieu, Lyotropic liquid crystals: structure and molecular motion, in: L. Liebert (Ed.), Solid-State Physics, supp. 14, Academic Press, New York, 1978, pp. 209–256.
[52] P.G. de Gennes, Dynamics of fluctuations in nematic liquid crystals, J. Chem. Phys. 51 (1969) 816–822.
[53] W. Helfrich, Elastic properties of lipid bilayers. Theory and possible experiments, Z. Naturforsch. 28c (1973) 693–703.
[54] H. Frauenfelder, G. Chen, J. Berendzen, P.W. Fenimore, H. Jansson, B.H. McMahon, I.R. Stroe, J. Swenson, R.D. Young, A unified model of protein dynamics, Proc. Natl. Acad. Sci. U.S.A. 106 (2009) 5129–5134.
[55] J.B. Klauda, R.M. Venable, J.A. Freites, J.W. O'Connor, D.J. Tobias, C. Mondragon-Ramirez, I. Voroboyov, A.D. MacKerell, R.W. Pastor, Update of the CHARMM all-atom additive force field for lipids: validation on six lipid types, J. Phys. Chem. B 114 (2010) 7830–7843.
[56] M. Bloom, NMR studies of membranes and whole cells, in: B. Maraviglia (Ed.), Physics of NMR Spectroscopy in Biology and Medicine, North-Holland Physics Publishing, New York, 1988, pp. 121–157.
[57] M. Bloom, C. Morrison, E. Sternin, J.L. Thewalt, Spin echoes and the dynamic properties of membranes, in: D.M.S. Bagguley (Ed.), Pulsed Magnetic Resonance: NMR, ESR, Optics, Clarendon Press, Oxford, 1992, pp. 274–316.
[58] R.G. Griffin, K. Beshah, R. Ebelhäuser, T.H. Huang, E.T. Olejniczak, D.M. Rice, D.J. Siminovitch, R.J. Wittebort, Deuterium NMR studies of dynamics in solids, in: G.J. Long, F. Grandjean (Eds.), The Time Domain in Surface and Structural Dynamics, Kluwer Academic Publishers, Dordrecht, 1988, pp. 81–105.
[59] M.F. Brown, J. Seelig, U. Häberlen, Structural dynamics in phospholipid bilayers from deuterium spin-lattice relaxation time measurements, J. Chem. Phys. 70 (1979) 5045–5053.
[60] J. Seelig, A. Seelig, Lipid conformation in model membranes and biological membranes, Q. Rev. Biophys. 13 (1980) 19–61.
[61] W.L. Hubbell, H.M. McConnell, Molecular motion in spin-labeled phospholipids and membranes, J. Am. Chem. Soc. 93 (1971) 314–326.
[62] H.M. McConnell, Molecular motion in biological membranes, in: L.J. Berliner (Ed.), Spin Labeling Theory and Applications, Academic Press, New York, 1976, pp. 525–560.
[63] R.R. Vold, Deuterium NMR studies of dynamics in solids and liquid crystals, in: R. Tycko (Ed.), Nuclear Magnetic Resonance Probes of Molecular Dynamics, Kluwer Academic Publishers, Dordrecht, 1994, pp. 27–112.
[64] U. Häberlen, High-Resolution NMR in Solids. Selective Averaging, Academic Press, New York, 1976.
[65] H.W. Spiess, Rotation of molecules and nuclear spin relaxation, in: P. Diehl, E. Fluck, R. Kosfeld (Eds.), NMR Basic Principles and Progress, vol. 15, Springer-Verlag, Heidelberg, 1978, pp. 55–214.
[66] M.F. Brown, S.I. Chan, Bilayer membranes: deuterium & carbon-13 NMR, in: D.M. Grant, R.K. Harris (Eds.), Encyclopedia of Nuclear Magnetic Resonance, vol. 2, Wiley, New York, 1996, pp. 871–885.
[67] J.D. Gross, D.E. Warschawski, R.G. Griffin, Dipolar recoupling in MAS NMR: a probe for segmental order in lipid bilayers, J. Am. Chem. Soc. 119 (1997) 796–802.
[68] M. Hong, K. Schmidt-Rohr, A. Pines, NMR measurement of signs and magnitudes of C–H dipolar couplings in lecithin, J. Am. Chem. Soc. 117 (1995) 3310–3311.
[69] S.V. Dvinskikh, V. Castro, D. Sandström, Efficient solid-state NMR methods for measuring heteronuclear dipolar couplings in unoriented lipid membrane systems, Phys. Chem. Chem. Phys. 7 (2005) 607–613.
[70] A.G. Lee, N.J.M. Birdsall, Y.K. Levine, J.C. Metcalfe, High resolution proton relaxation studies of lecithin, Biochim. Biophys. Acta 255 (1972) 43–56.
[71] M. Kainosho, P.A. Kroon, R. Lawaczek, N.O. Petersen, S.I. Chan, Chain length dependence of the ^{1}H NMR relaxation rates in bilayer vesicles, Chem. Phys. Lipids 21 (1978) 59–68.
[72] G.W. Feigenson, S.I. Chan, Nuclear magnetic relaxation behavior of lecithin multilayers, J. Am. Chem. Soc. 96 (1974) 1312–1319.
[73] S.I. Chan, G.W. Feigenson, C.H.A. Seiter, Nuclear relaxation studies of lecithin bilayers, Nature 231 (1971) 110–112.
[74] E. Oldfield, J.L. Bowers, J. Forbes, High-resolution proton and carbon-13 NMR of membranes: why sonicate? Biochemistry 26 (1987) 6919–6923.
[75] Y.K. Levine, N.J.M. Birdsall, A.G. Lee, J.C. Metcalfe, ^{13}C nuclear magnetic resonance relaxation measurements of synthetic lecithins and the effect of spin-labeled lipids, Biochemistry 11 (1972) 1416–1421.
[76] J.R. Lyerla Jr., H.M. McIntyre, D.A. Torchia, A ^{13}C nuclear magnetic resonance study of alkane motion, Macromolecules 7 (1974) 11–14.
[77] J.R. Lyerla Jr., G.C. Levy, Carbon-13 nuclear spin relaxation, in: G.C. Levy (Ed.), Topics in Carbon-13 NMR Spectroscopy, vol. 1, John Wiley & sons, New York, 1974, pp. 79–148.
[78] J.B. Klauda, N.V. Eldho, K. Gawrisch, B.R. Brooks, R.W. Pastor, Collective and noncollective models of NMR relaxation in lipid vesicles and multilayers, J. Phys. Chem. B 112 (2008) 5924–5929.
[79] E. Oldfield, M. Meadows, D. Rice, R. Jacobs, Spectroscopic studies of specifically deuterium labeled membrane systems. Nuclear magnetic resonance investigation of the effects of cholesterol in model systems, Biochemistry 17 (1978) 2727–2740.
[80] R.A. Haberkorn, R.G. Griffin, M.D. Meadows, E. Oldfield, Deuterium nuclear magnetic resonance investigation of the dipalmitoyl lecithin–cholesterol–water system, J. Am. Chem. Soc. 99 (1977) 7353–7355.
[81] J. Seelig, A. Seelig, Deuterium magnetic resonance studies of phospholipid bilayers, Biochem. Biophys. Res. Commun. 57 (1974) 406–411.
[82] J. Seelig, W. Niederberger, Deuterium-labeled lipids as structural probes in liquid crystalline bilayers. Deuterium magnetic resonance study, J. Am. Chem. Soc. 96 (1974) 2069–2072.
[83] A. Seelig, J. Seelig, The dynamic structure of fatty acyl chains in a phospholipid bilayer measured by deuterium magnetic resonance, Biochemistry 13 (1974) 4839–4845.
[84] P.J. Flory, Statistical Mechanics of Chain Molecules, Interscience, New York, 1969.
[85] S. Marčelja, Chain ordering in liquid crystals. II. Structure of bilayer membranes, Biochim. Biophys. Acta 367 (1974) 165–176.
[86] H. Schindler, J. Seelig, Deuterium order parameters in relation to thermodynamic properties of a phospholipid bilayer. A statistical mechanical interpretation, Biochemistry 14 (1975) 2283–2287.
[87] J.-P. Meraldi, J. Schlitter, A statistical mechanical treatment of fatty acyl chain order in phospholipid bilayers and correlation with experimental data. A. Theory, Biochim. Biophys. Acta 645 (1981) 183–192.
[88] J.-P. Meraldi, J. Schlitter, A statistical mechanical treatment of fatty acyl chain order in phospholipid bilayers and correlation with experimental data. B. Dipalmitoyl-3-*sn*-phosphatidylcholine, Biochim. Biophys. Acta 645 (1981) 193–210.
[89] D.W.R. Gruen, Statistical thermodynamics of alkyl chain conformations in lipid bilayers, Chem. Phys. Lipids 30 (1982) 105–120.
[90] D.W.R. Gruen, A model for the chains in amphiphilic aggregates. 1. Comparison with a molecular dynamics simulation of a bilayer, J. Phys. Chem. 89 (1985) 146–153.
[91] D.W.R. Gruen, A model for the chains in amphiphilic aggregates. 2. Thermodynamic and experimental comparisons for aggregates of different shape and size, J. Phys. Chem. (1985) 153–163.
[92] A. Salmon, S.W. Dodd, G.D. Williams, J.M. Beach, M.F. Brown, Configurational statistics of acyl chains in polyunsaturated lipid bilayers from ^{2}H NMR, J. Am. Chem. Soc. 109 (1987) 2600–2609.

[93] R.L. Thurmond, Average and dynamic properties of membrane lipids studied by deuterium NMR spectroscopy, Ph.D. Dissertation, University of Arizona (1992).
[94] A. Salmon, Determination of acyl chain ordering and dynamics in polyunsaturated bilayers by deuterium NMR, Ph.D. Dissertation, University of Virginia (1988).
[95] S.W. Dodd, Deuterium nuclear magnetic resonance studies of saturated phospholipid bilayers in the liquid-crystalline state, M.S. Thesis, University of Virginia (1987).
[96] G.D. Williams, Molecular dynamics of biological membranes from carbon-13 and deuterium nuclear magnetic resonance relaxation studies of synthetic lipid bilayers, Ph.D. Dissertation, University of Virginia (1987).
[97] H.I. Petrache, K. Tu, J.F. Nagle, Analysis of simulated NMR order parameters for lipid bilayer structure determination, Biophys. J. 76 (1999) 2479–2487.
[98] S. Jo, T. Kim, V.G. Iyer, W. Im, CHARMM-GUI: a web-based graphical user interface for CHARMM, J. Comput. Chem. 29 (2008) 1859–1865.
[99] S.E. Feller, R.W. Pastor, On simulating lipid bilayers with an applied surface tension: periodic boundary conditions and undulations, Biophys. J. 71 (1996) 1350–1355.
[100] S.E. Feller, R.M. Venable, R.W. Pastor, Computer simulation of a DPPC phospholipid bilayer: stuctural changes as a function of molecular surface area, Langmuir 13 (1997) 6555–6561.
[101] L.S. Vermeer, B.L. de Groot, V. Reat, A. Milon, J. Czaplicki, Acyl chain order parameter profiles in phopholipid bilayers: computation from molecular dynamics simulations and comparison with ^{2}H NMR experiments, Eur. Biophys. J. 36 (2007) 919–931.
[102] B.J. Hardy, R.W. Pastor, Conformational sampling of hydrocarbon and lipid chains in an orienting potential, J. Comput. Chem. 15 (1993) 208–226.
[103] C.P. Slichter, Principles of Magnetic Resonance, Third Edition, Springer-Verlag, Heidelberg, 1990.
[104] J.-M. Bonmatin, I.C.P. Smith, H.C. Jarrell, D.J. Siminovitch, Orientation dependence of ^{2}H NMR spin-lattice relaxation rates for cholesterol in macroscopically oriented multibilayers, J. Am. Chem. Soc. 110 (1988) 8693–8695.
[105] M.F. Brown, Anisotropic nuclear spin relaxation of cholesterol in phospholipid bilayers, Mol. Phys. 71 (1990) 903–908.
[106] A.G. Redfield, The theory of relaxation processes, Adv. Magn. Reson. 1 (1965) 1–32.
[107] Y.K. Levine, P. Partington, G.C.K. Roberts, N.J.M. Birdsall, A.G. Lee, J.C. Metcalfe, ^{13}C nuclear magnetic relaxation times and models for chain motion in lecithin vesicles, FEBS Lett. 23 (1972) 203–207.
[108] B.M. Fung, T.H. Martin, Magnetic relaxation in the lecithin-D_2O system, J. Am. Chem. Soc. 97 (1975) 5719–5723.
[109] M.F. Brown, Deuterium relaxation and molecular dynamics in lipid bilayers, J. Magn. Reson. 35 (1979) 203–215.
[110] J.H. Davis, Deuterium magnetic resonance study of the gel and liquid crystalline phases of dipalmitoylphosphatidylcholine, Biophys. J. 27 (1979) 339–358.
[111] D.J. Siminovitch, M.J. Ruocco, E.T. Olejniczak, S.K. Das Gupta, R.G. Griffin, Anisotropic spin-lattice relaxation in lipid bilayers: a solid state ^{2}H NMR lineshape study, Chem. Phys. Lett. 119 (1985) 251–255.
[112] M.P.N. Gent, J.H. Prestegard, Comparison of ^{13}C spin-lattice relaxation times in phospholipid vesicles and multilayers, Biochem. Biophys. Res. Commun. 58 (1974) 549–555.
[113] M.P. Milburn, K.R. Jeffrey, Dynamics of the phosphate group in phospholipid bilayers. A ^{31}P nuclear relaxation time study, Biophys. J. 52 (1987) 791–799.
[114] V. Viti, M. Minetti, ^{31}P NMR study of head group behavior in sonicated phosphatidylcholine liposomes in the gel and liquid state, Chem. Phys. Lipids 28 (1981) 215–225.
[115] R.W. Fisher, T. James, Lateral diffusion of the phospholipid molecule in dipalmitoylphosphatidylcholine bilayers. An investigation using nuclear spin-lattice relaxation time in the rotating frame, Biochemistry 17 (1978) 1177–1183.
[116] A.C. McLaughlin, F. Podo, J.K. Blaise, Temperature and frequency dependence of longitudinal proton relaxation times in sonicated lecithin dispersions, Biochim. Biophys. Acta (1973) 109–121.
[117] F. Noack, NMR field-cycling spectroscopy: principles and applications, Prog. Nucl. Magn. Reson. Spectrosc. 18 (1986) 171–276.
[118] S. Meiboom, D. Gill, Modified spin-echo method for measuring nuclear relaxation times, Rev. Sci. Instrum. 29 (1958) 688–691.
[119] H.Y. Carr, E.M. Purcell, Effects of diffusion on free precession in NMR experiments, Phys. Rev. 94 (1954) 630–638.
[120] A.G. Palmer III, C.D. Kroenke, J.P. Loria, Nuclear magnetic resonance methods for quantifying microsecond-to-millisecond motions in biological macromolecules, Meth. Enzymol. 339 (2001) 204–238.
[121] M. Bloom, E. Sternin, Transverse nuclear spin relaxation in phospholipid bilayer membranes, Biochemistry 26 (1987) 2101–2105.
[122] R. Kimmich, N. Fatkullin, H.W. Weber, S. Stapf, Nuclear spin-lattice relaxation and theories of polymer dynamics, J. Non-Cryst. Solids 172–174 (1994) 689–697.
[123] F. Noack, M. Notter, W. Weiss, Relaxation dispersion and zero-field spectroscopy of thermotropic and lyotropic liquid crystals by fast field-cycling N.M.R. Liquid Cryst. 3 (1988) 907–925.
[124] V.N. Sivanandam, J. Cai, A.G. Redfield, M.F. Roberts, Phosphatidylcholine "wobble" in vesicles assessed by ^{13}C field cycling NMR spectroscopy, J. Am. Chem. Soc. 10 (2009) 3420–3421.
[125] M.F. Roberts, A.G. Redfield, High-resolution ^{31}P field cycling NMR as a probe of phospholipid dynamics, J. Am. Chem. Soc. 42 (2004) 13765–13777.
[126] R. Kimmich, E. Anoardo, Field-cycling NMR relaxometry, Prog. Nucl. Magn. Reson. Spectrosc. 44 (2004) 257–320.
[127] L.E. Kay, D.A. Torchia, A. Bax, Backbone dynamics of proteins as studied by ^{15}N inverse detected heteronuclear NMR spectroscopy: application to staphlococcal nuclease, Biochemistry 28 (1989) 8972–8979.
[128] J. Cavanaugh, W.J. Fairbrother, A.G. Palmer III, N.J. Skelton, M. Rance, Protein NMR Spectroscopy: Principles and Practice, Second Edition, Academic Press, New York, 2006.
[129] P. Vallurapalli, D.F. Hansen, L.E. Kay, Structures of invisible, excited protein states by relaxation dispersion NMR spectroscopy, Proc. Natl. Acad. Sci. U.S.A. 105 (2008) 11766–11771.
[130] K. Henzler-Wildman, D. Kern, Dynamic personalities of proteins, Nature 450 (2007) 964–972.
[131] D.A. Torchia, Solid state NMR studies of protein internal dynamics, Annu. Rev. Biophys. Bioeng. 13 (1984) 125–144.
[132] H.J. Dyson, P.E. Wright, Insights into protein folding from NMR, Annu. Rev. Phys. Chem. 47 (1996) 369–395.
[133] A.A. Nevzorov, Dynamic and equilibrium properties of membrane constituents and nucleic acids from deuterium NMR spectroscopy, Ph.D. Dissertation, University of Arizona (1998).
[134] T.M. Alam, Molecular dynamics in lipid bilayers: anisotropic diffusion in an odd restoring potential, Biophys. J. 64 (1993) 1681–1690.
[135] T.P. Trouard, T.M. Alam, M.F. Brown, Angular dependence of deuterium spin-lattice relaxation rates of macroscopically oriented dilaurylphosphatidylcholine in the liquid-crystalline state, J. Chem. Phys. 101 (1994) 5229–5261.
[136] P.-L. Nordio, U. Segre, Rotational dynamics, in: G.R. Luckhurst, G.W. Gray (Eds.), The Molecular Physics of Liquid Crystals, Academic Press, New York, 1979, pp. 411–426.
[137] J.H. Freed, Stochastic-molecular theory of spin-relaxation for liquid crystals, J. Chem. Phys. 66 (1977) 4183–4199.
[138] R.J. Pace, S.I. Chan, Molecular motions in lipid bilayers. I. Statistical mechanical model of acyl chain motion, J. Chem. Phys. 76 (1982) 4217–4227.
[139] R.J. Pace, S.I. Chan, Molecular motions in lipid bilayers. II. Magnetic resonance of multilamellar and vesicle systems, J. Chem. Phys. 76 (1982) 4228–4240.
[140] R.J. Pace, S.I. Chan, Molecular motions in lipid bilayers. III. Lateral and transverse diffusion in bilayers, J. Chem. Phys. 76 (1982) 4241–4247.
[141] G. Althoff, N.J. Heaton, G. Gröbner, R.S. Prosser, G. Kothe, NMR relaxation study of collective motions and viscoelastic properties in biomembranes, Colloid Surf. A 115 (1996) 31–37.
[142] J. Stohrer, G. Gröbner, D. Reimer, K. Weisz, C. Mayer, G. Kothe, Collective lipid motions in bilayer membranes studied by transverse deuteron spin relaxation, J. Chem. Phys. 95 (1991) 672–678.
[143] J. Struppe, F. Noack, G. Klose, NMR study of collective motions and bending rigidity in multilamellar system of lipid and surfactant bilayers, Z. Naturforsch. 52 (1997) 681–694.
[144] M.F. Brown, J.H. Davis, Orientation and frequency dependence of the deuterium spin-lattice relaxation in multilamellar phospholipid dispersions: implications for dynamic models of membrane structure, Chem. Phys. Lett. 79 (1981) 431–435.
[145] E. Rommel, F. Noack, P. Meier, G. Kothe, Proton spin relaxation dispersion studies of phospholipid membranes, J. Phys. Chem. 92 (1988) 2981–2987.
[146] A.G. Redfield, Shuttling device for high-resolution measurements of relaxation and related phenomena in solution at low field, using a shared commercial 500 MHz NMR instrument, Magn. Reson. Chem. 41 (2003) 753–768.
[147] P. Pincus, Nuclear relaxation in a nematic liquid crystal, Solid State Commun. 7 (1969) 415–417.
[148] G. Williams, Molecular motion in glass-forming systems, J. Non-Cryst. Solids 131 (1991) 1–12.
[149] G. Williams, D.C. Watts, Non-symmetrical dielectric relaxation behavior arising from a simple empirical decay function, Trans. Faraday Soc. 66 (1970) 80–85.
[150] R. Hilfer, Analytical representations for relaxation functions in glasses, J. Non-Cryst. Solids 305 (2002) 122–126.
[151] P.A. Beckmann, Spectral densities and nuclear spin relaxation in solids, Phys. Rep. 171 (1988) 85–128.
[152] K. Weisz, G. Gröbner, C. Mayer, J. Stohrer, G. Kothe, Deuteron nuclear magnetic resonance study of the dynamic organization of phospholipid/cholesterol bilayer membranes: molecular properties and viscoelastic behavior, Biochemistry 31 (1992) 1100–1112.
[153] M.F. Brown, Unified picture for spin-lattice relaxation of lipid bilayers and biomembranes, J. Chem. Phys. 80 (1984) 2832–2836.
[154] G. Althoff, D. Frezzato, M. Vilfan, O. Stauch, R. Schubert, I. Vilfan, G.J. Moro, G. Kothe, Transverse nuclear spin relaxation studies of viscoelastic properties of membrane vesicles. I. Theory, J. Phys. Chem. B 106 (2002) 5506–5516.
[155] G. Althoff, O. Stauch, M. Vilfan, D. Frezzato, G.J. Moro, P. Hauser, R. Schubert, G. Kothe, Transverse nuclear spin relaxation studies of viscoelastic properties of membrane vesicles. II. Experimental results, J. Phys. Chem. B 106 (2002) 5517–5526.
[156] J. Seelig, J.L. Browning, General features of phospholipid conformation in membranes, FEBS Lett. 92 (1978) 41–44.
[157] M.F. Brown, R.L. Thurmond, S.W. Dodd, D. Otten, K. Beyer, Elastic deformation of membrane bilayers probed by deuterium NMR relaxation, J. Am. Chem. Soc. 124 (2002) 8471–8484.
[158] J.H. Davis, K.R. Jeffrey, The temperature dependence of chain disorder in potassium palmitate-water. A deuterium NMR study, Chem. Phys. Lipids 20 (1977) 87–104.
[159] D.C. Douglass, G.P. Jones, Nuclear magnetic relaxation of *n*-alkanes in the rotating frame, J. Chem. Phys. 45 (1966) 956–963.
[160] J. Charvolin, P. Rigny, Proton relaxation study of paraffin chain motions in a lyotropic liquid crystal, J. Chem. Phys. 58 (1973) 3999–4008.

[161] K.R. Jeffrey, T.C. Wong, E.E. Burnell, M.J. Thompson, T.P. Higgs, N.R. Chapman, Molecular motion in the lyotropic liquid crystal system containing potassium palmitate: a study of proton spin-lattice relaxation times, J. Magn. Reson. 36 (1979) 151–171.
[162] J.H. Davis, K.R. Jeffrey, M. Bloom, Spin-lattice relaxation as a function of chain position in perdeuterated potassium palmitate, J. Magn. Reson. 29 (1978) 191–199.
[163] K.R. Jeffrey, T.C. Wong, A.P. Tulloch, Molecular dynamics in lamellar lyotropic mesophases with ordered and disordered hydrocarbon chains. I. A study of the deuteron N.M.R. spectra, Mol. Phys. 52 (1984) 289–306.
[164] K.R. Jeffrey, T.C. Wong, A.P. Tulloch, Molecular dynamics in lamellar lyotropic mesophases with ordered and disordered hydrocarbon chains. II. A study of the deuteron nuclear magnetic resonance relaxation times, Mol. Phys. 52 (1984) 307–318.
[165] W. Kühner, E. Rommel, F. Noack, Proton spin relaxation study of molecular motions in the lyotropic liquid crystalline system potassium-laurate water, Z. Naturforsch. 42 (1987) 127–135.
[166] G. Lindblom, G. Orädd, NMR studies of translational diffusion in lyotropic liquid crystals and in lipid membranes, Prog. Nucl. Magn. Reson. Spectrosc. 26 (1994) 483–515.
[167] M.F. Brown, A.A. Ribeiro, G.D. Williams, New view of lipid bilayer dynamics from ^{2}H and ^{13}C NMR relaxation time measurements, Proc. Natl. Acad. Sci. U.S.A. 80 (1983) 4325–4329.
[168] R.M. Venable, Y. Zhang, B.J. Hardy, R.W. Pastor, Molecular dynamics simulations of a lipid bilayer and of hexadecane: an investigation of membrane fluidity, Science 262 (1993) 223–226.
[169] R.W. Pastor, R.M. Venable, Brownian dynamics simulation of a lipid chain in a membrane bilayer, J. Chem. Phys. 89 (1988) 1112–1127.
[170] R.W. Pastor, R.M. Venable, M. Karplus, A. Szabo, A simulation based model of NMR T_1 relaxation in lipid bilayer vesicles, J. Chem. Phys. 89 (1988) 1128–1140.
[171] R.W. Pastor, R.M. Venable, M. Karplus, Model for the structure of the lipid bilayer, Proc. Natl. Acad. Sci. U.S.A. 88 (1991) 892–896.
[172] D.P. Tieleman, S.J. Marrink, H.J.C. Berendsen, A computer perspective of membranes: molecular dynamics studies of lipid bilayer systems, Biochim. Biophys. Acta 1331 (1997) 235–270.
[173] G.S. Ayton, G.A. Voth, Hybrid coarse-graining approach for lipid bilayers at large length and time scales, J. Phys. Chem. B 113 (2009) 4413–4424.
[174] J.B. Klauda, B.R. Brooks, A.D. MacKerell Jr., R.M. Venable, R.W. Pastor, An ab initio study on the torsional surface of alkanes and its effect on molecular simulations of alkanes and a DPPC bilayer, J. Phys. Chem. B 109 (2005) 5300–5311.
[175] W. Helfrich, Steric interaction of fluid membranes in multilayer systems, Z. Naturforsch. 33a (1978) 305–315.
[176] J. Wohlert, O. Edholm, Dynamics in atomistic simulations of phospholipid membranes: nuclear magnetic resonance relaxation rates and lateral diffusion, J. Chem. Phys. 125 (2006) 204703-1–20473-10.
[177] G.S. Ayton, J.L. McWhirter, G.A. Voth, A second generation mesoscopic lipid bilayer model: connections to field-theory description of membranes and nonlocal hydrodynamics, J. Chem. Phys. 124 (2006) 064906-1–064906-12.
[178] H.J. Risselada, S.J. Marrink, The molecular face of lipid rafts in model membranes, Proc. Natl. Acad. Sci. U.S.A. 105 (2008) 17367–17372.
[179] F. Castro-Romn, R.W. Benz, S.H. White, D.J. Tobias, Investigation of finite system-size effects in molecular dynamics simulations of lipid bilayers, J. Phys. Chem. B 110 (2006) 24157–24164.
[180] R.G. Griffin, Observation of the effect of water on the ^{31}P nuclear magnetic resonance spectra of dipalmitoyllecithin, J. Am. Chem. Soc. 98 (1976) 851–853.
[181] P.R. Cullis, B. de Kruijff, Polymorphic phase behaviour of lipid mixtures as detected by ^{31}P-NMR, Biochim. Biophys. Acta 507 (1978) 207–218.
[182] A. Blume, R.G. Griffin, Carbon-13 and deuterium nuclear magnetic resonance study of the interaction of cholesterol with phosphatidylethanolamine, Biochemistry 21 (1982) 6230–6242.
[183] M.F. Brown, J. Seelig, Ion-induced changes in head group conformation of lecithin bilayers, Nature 269 (1977) 721–723.
[184] D.J. Siminovitch, M.F. Brown, K.R. Jeffrey, ^{14}N NMR of lipid bilayers: effects of ions and anesthetics, Biochemistry 23 (1984) 2412–2420.
[185] D.J. Siminovitch, M. Rance, K.R. Jeffrey, M.F. Brown, The quadrupolar spectrum of a spin $I=1$ in a lipid bilayer in the presence of paramagnetic ions, J. Magn. Reson. 58 (1984) 62–75.
[186] M. Bloom, F. Linseisen, J. Lloyd-Smith, M.A. Crawford, Insights from NMR on the functional role of polyunsaturated lipids in the brain, in: B. Maraviglia (Ed.), Magnetic Resonance and Brain Function, Proc. International School of Physics Enrico Fermi, Varenna, Italy, 1998.
[187] C. Mayer, G. Gröbner, K. Müller, K. Weisz, G. Kothe, Orientation-dependent deuteron spin-lattice relaxation times in bilayer membranes: characterization of the overall lipid motion, Chem. Phys. Lett. 165 (1990) 155–161.
[188] D.E. Warschawski, P.F. Deveaux, Order parameters of unsaturated phospholipids in membranes and the effect of cholesterol: a ^{1}H–^{13}C solid-state NMR study at natural abundance, Eur. Biophys. J. 34 (2005) 987–996.
[189] K. Rajamoorthi, H.I. Petrache, T.J. McIntosh, M.F. Brown, Packing and viscoelasticity of polyunsaturated ω-3 and ω-6 lipid bilayers as seen by ^{2}H NMR and X-ray diffraction, J. Am. Chem. Soc. 127 (2005) 1576–1588.
[190] K. Rajamoorthi, M.F. Brown, Bilayers of arachidonic acid containing phospholipids studied by ^{2}H and ^{31}P NMR spectroscopy, Biochemistry 30 (1991) 4204–4212.
[191] H.I. Petrache, A. Salmon, M.F. Brown, Structural properties of docosahexaenoyl phosphatidylcholine bilayers investigated by solid-state ^{2}H NMR spectroscopy, J. Am. Chem. Soc. 123 (2001) 12611–12622.
[192] D. Huster, K. Arnold, K. Gawrisch, Influence of docosahexaenoic acid and cholesterol on lateral lipid organization in phospholipid mixtures, Biochemistry 37 (1998) 17299–17308.
[193] H. Binder, K. Gawrisch, Dehydration induces lateral expansion of polyunsaturated 18:0–22:6 phosphatidylcholine in a new lamellar phase, Biophys. J. 81 (2001) 969–982.
[194] J.A. Barry, T.P. Trouard, A. Salmon, M.F. Brown, Low-temperature ^{2}H NMR spectroscopy of phospholipid bilayers containing docosahexaenoyl (22:6ω3) chains, Biochemistry 30 (1991) 8386–8394.
[195] M.F. Brown, S.W. Dodd, A. Salmon, Deuterium NMR spectroscopy of saturated and polyunsaturated lipid bilayers, in: A. Kotyk, et al., (Eds.), Highlights of Modern Biochemistry, VSP International, Zeist, 1989, pp. 725–734.
[196] J.E. Baenziger, H.C. Jarrell, R.J. Hill, I.C.P. Smith, Average structural and motional properties of a diunsaturated acyl chain in a lipid bilayer: effects of two *cis*-unsaturated double bonds, Biochemistry 30 (1991) 894–903.
[197] B. Koenig, H. Strey, K. Gawrisch, Membrane lateral compressibility determined by NMR and X-ray diffraction: effect of acyl chain polyunsaturation, Biophys. J. 73 (1997) 1954–1966.
[198] L.L. Holte, F. Separovic, K. Gawrisch, Nuclear magnetic resonance investigation of hydrocarbon chain packing in bilayers of polyunsaturated phospholipids, Lipids 31 (1996) S199–S203.
[199] T. Huber, K. Rajamoorthi, V.F. Kurze, K. Beyer, M.F. Brown, Structure of docosahexaenoic acid-containing phospholipid bilayers as studied by ^{2}H NMR and molecular dynamics simulations, J. Am. Chem. Soc. 124 (2002) 298–309.
[200] N.V. Eldho, S.E. Feller, S. Tristram-Nagle, I.V. Polozov, K. Gawrisch, Polyunsaturated docohexaenoic vs docosapentaenoic acid — differences in lipid matrix from the loss of one double bond, J. Am. Chem. Soc. 125 (2003) 6409–6421.
[201] J. Zajicek, J.F. Ellena, G.D. Williams, M.A. Khadim, M.F. Brown, Molecular dynamics of vesicles of unsaturated phosphatidylcholines studied by ^{13}C NMR spin-lattice relaxation, Collect. Czech. Chem. Commun. 60 (1995) 719–735.
[202] H. Hauser, I. Pascher, R.H. Pearson, S. Sundell, Preferred conformation and molecular packing of phosphatidylethanolamine and phosphatidylcholine, Biochim. Biophys. Acta 650 (1981) 21–51.
[203] R.L. Thurmond, G. Lindblom, M.F. Brown, Curvature, order, and dynamics of lipid hexagonal phases studied by deuterium NMR spectroscopy, Biochemistry 32 (1993) 5394–5410.
[204] J. Seelig, H.-U. Gally, Investigation of phosphatidylethanolamine bilayers by deuterium and phosphorus-31 nuclear magnetic resonance, Biochemistry 15 (1976) 5199–5204.
[205] D. Marsh, A. Watts, I.C.P. Smith, Dynamic structure and phase behavior of dimyristoylphosphatidylethanolamine bilayers studied by deuterium nuclear magnetic resonance, Biochemistry 22 (1983) 3023–3026.
[206] S.J. Kohler, M.P. Klein, ^{31}P nuclear magnetic resonance chemical shielding tensors of phosphorylethanolamine, lecithin and related compounds. Applications to head-group motion in model membranes, Biochemistry 15 (1976) 967–973.
[207] A.M. Thayer, S.J. Kohler, Phosphorus-31 spectra characteristic of hexagonal and isotropic phospholipid phases generated from phosphatidylethanolamine in the bilayer phase, Biochemistry 20 (1981) 6831–6834.
[208] S.M. Gruner, P.R. Cullis, M.J. Hope, C.P.S. Tilcock, Lipid polymorphism: the molecular basis of nonbilayer phases, Annu. Rev. Biophys. Biophys. Chem. 14 (1985) 211–238.
[209] H.-U. Gally, W. Niederberger, J. Seelig, Conformation and motion of the choline head group in bilayers of dipalmitoyl-3-*sn*-phosphatidylcholine, Biochemistry 14 (1975) 3647–3652.
[210] A.C. McLaughlin, P.R. Cullis, M.A. Hemminga, D.I. Hoult, G.K. Radda, G.A. Ritchie, P.J. Seeley, R.E. Richards, Application of ^{31}P NMR to model and biological membrane systems, FEBS Lett. 57 (1975) 213–218.
[211] R.G. Griffin, L. Powers, P.S. Pershan, Head group conformation in phospholipids: a phosphorus-31 nuclear magnetic resonance study of oriented monodomain dipalmitoylphosphatidylcholine bilayers, Biochemistry 17 (1978) 2718–2722.
[212] J. Seelig, ^{31}P nuclear magnetic resonance and the head group structure of phospholipids in membranes, Biochim. Biophys. Acta 515 (1978) 105–140.
[213] E.J. Dufourc, C. Mayer, J. Stohrer, G. Althoff, G. Kothe, Dynamics of phosphate head groups in biomembranes. Comprehensive analysis using phosphorus-31 nuclear magnetic resonance lineshape and relaxation time measurements, Biophys. J. 61 (1992) 42–57.
[214] R.L. Thurmond, G. Lindblom, M.F. Brown, Effect of bile salts on monolayer curvature of a phosphatidylethanolamine/water model membrane system, Biophys. J. 60 (1991) 728–732.
[215] D.B. Fenske, H.C. Jarrell, Y. Guo, S.W. Hui, Effect of unsaturated phosphatidylethanolamine on the chain order profile of bilayers at the onset of the hexagonal phase transition. A ^{2}H NMR study, Biochemistry 29 (1990) 11222–11229.
[216] B. Perly, I.C.P. Smith, H.C. Jarrell, Acyl chain dynamics of phosphatidylethanolamines containing oleic acid and dihydrosterculic acid: ^{2}H NMR relaxation studies, Biochemistry 24 (1985) 4659–4665.
[217] P.-O. Eriksson, L. Rilfors, G. Lindblom, G. Arvidson, Multicomponent spectra from ^{31}P NMR studies of the phase equilibria in the system dioleoylphosphatidylcholine-dioleoylphosphatidylethanolamine-water, Chem. Phys. Lipids 37 (1985) 357–371.
[218] C.P.S. Tilcock, P.R. Cullis, The polymorphic phase behaviour and miscibility properties of synthetic phosphatidylethanolamines, Biochim. Biophys. Acta 684 (1982) 212–218.
[219] R.L. Thurmond, S.W. Dodd, M.F. Brown, Molecular areas of phospholipids as determined by ^{2}H NMR spectroscopy: comparison of phosphatidylethanolamines and phosphatidylcholines, Biophys. J. 59 (1991) 108–113.
[220] R.E. Redfern, D. Redfern, M.L.M. Furgason, M. Munson, A.H. Ross, A. Gericke, PTEN phosphatase selectively binds phosphoinositides and undergoes structural changes, Biochemistry 47 (2008) 2162–2171.

[221] R. Nayar, S.L. Schmid, M.J. Hope, P.R. Cullis, Structural preferences of phosphatidylinositol and phosphatidylinositol-phosphatidylethanolamine model membranes, Biochim. Biophys. Acta 688 (1982) 169–176.
[222] E.E. Kooijman, K.E. King, M. Gangoda, A. Gericke, Ionization properties of phosphatidylinositol polyphosphates in mixed model membranes, Biochemistry 48 (2009) 9360–9371.
[223] J.P. Bradshaw, R.J. Bushby, C.C.D. Giles, M.R. Saunders, Orientation of the headgroup of phosphatidylinositol in a model biomembrane as determined by neutron diffraction, Biochemistry 38 (1999) 8393–8401.
[224] M.R. Gryk, R.S. Abseher, B. Simon, M. Nilges, H. Oschkinat, Heteronuclear relaxation study of the PH domain of beta-spectrin: restriction of loop motions upon binding inositol trisphosphate, J. Mol. Biol. 280 (1998) 879–896.
[225] D. Raucher, T. Stauffer, W. Chen, K. Shen, S. Guo, J.D. York, M.P. Sheetz, T. Meyer, Phosphatidylinositol 4, 5-bisphosphate functions as a second messenger that regulates cytoskeleton–plasma membrane adhesion, Cell 100 (2000) 221–228.
[226] J.L. Browning, J. Seelig, Bilayers of phosphatidylserine: a deuterium and phosphorus nuclear magnetic resonance study, Biochemistry 19 (1980) 1262–1270.
[227] M. Roux, M. Bloom, Calcium binding by phosphatidylserine headgroups. Deuterium NMR study, Biophys. J. 60 (1991) 38–44.
[228] M. Roux, J.-M. Neumann, Deuterium NMR study of headgroup deuterated phosphatidylserine in pure and binary phospholipid bilayers. Interactions with monovalent cations Na^+ and Li^+, FEBS Lett. 199 (1986) 33–38.
[229] M. Roux, J.-M. Neumann, M. Bloom, P.F. Devaux, ^2H and ^{31}P NMR studies of pentalysine interaction with headgroup deuterated phosphatidylcholine and phosphatidylserine, Eur. Biophys. J. 16 (1988) 267–273.
[230] H.L. Casal, H.H. Mantsch, F. Paltauf, H. Hauser, Infrared and ^{31}P NMR studies of the effect of Li^+ and Ca^{2+} on phosphatidylserine, Biochim. Biophys. Acta 919 (1987) 275–286.
[231] M.J. Hope, P.R. Cullis, Effects of divalent cations and pH on phosphatidylserine model membranes: a ^{31}P NMR study, Biochem. Biophys. Res. Commun. 92 (1980) 846–852.
[232] A.I.P.M. de Kroon, J.W. Timmermans, J.A. Killian, B. de Kruijff, The pH dependence of headroup and acyl chain structure and dynamics of phosphatidylserine, studied by ^2H-NMR, Chem. Phys. Lipids 54 (1990) 33–42.
[233] C.P.S. Tilcock, P.R. Cullis, The polymorphic phase behaviour of mixed phosphatidylserine-phosphatidylethanolamine model system as detected by ^{31}P-NMR. Effects of divalent cations and pH, Biochim. Biophys. Acta 641 (1980) 189–201.
[234] M. Auger, D. Carrier, I.C.P. Smith, H.C. Jarrell, Elucidation of motional modes in glycoglycerolipid bilayers. A ^2H NMR relaxation and line-shape study, J. Am. Chem. Soc. 112 (1990) 1373–1381.
[235] P. Ram, J.H. Prestegard, Head-group orientation of a glycolipid analogue from deuterium NMR data, J. Am. Chem. Soc. 110 (1988) 2383–2388.
[236] B. Bechinger, P.M. Macdonald, J. Seelig, Deuterium NMR studies of the interactions of polyhydroxyl compounds and of glycolipids with lipid model membranes, Biochim. Biophys. Acta 943 (1988) 381–385.
[237] F. Adebodun, J. Chung, B. Montez, E. Oldfield, X. Shan, Spectroscopic studies of lipids and biological membranes: carbon-13 and proton magic-angle sample-spinning nuclear magnetic resonance study of glycolipid-water systems, Biochemistry 31 (1992) 4502–4509.
[238] M.J. Ruocco, D.J. Siminovitch, J.R. Long, S.K. Das Gupta, R.G. Griffin, ^2H and ^{13}C nuclear magnetic resonance study of N-palmitoylgalactosylsphingosine (cerebroside)/cholesterol bilayers, Biophys. J. 71 (1996) 1776–1788.
[239] D.J. Siminovitch, K.R. Jeffrey, Orientational order in the choline headgroup of sphingomyelin: a ^{14}N-NMR study, Biochim. Biophys. Acta 645 (1981) 270–278.
[240] P.L. Yeagle, W.C. Hutton, R.B. Martin, Sphingomyelin multiple phase behavior as revealed by multinuclear magnetic resonance spectroscopy, Biochemistry 17 (1978) 5745–5750.
[241] M.R. Morrow, D. Singh, D. Lu, C.W.M. Grant, Glycosphingolipid phase behaviour in unsaturated phosphatidylcholine bilayers: a ^2H NMR study, Biochim. Biophys. Acta 1106 (1992) 85–93.
[242] M.R. Morrow, D. Singh, D. Lu, C.W.M. Grant, Glycosphingolipid acyl chain orientational order in unsaturated phosphatidylcholine bilayers, Biophys. J. 64 (1993) 654–664.
[243] J.B. Speyer, R.T. Weber, S.K. Das Gupta, R.G. Griffin, Anisotropic ^2H NMR spin-lattice relaxation in L_α-phase cerebroside bilayers, Biochemistry 28 (1989) 9569–9574.
[244] D.J. Siminovitch, M.J. Ruocco, E.T. Olejniczak, S.K. Das Gupta, R.G. Griffin, Anisotropic ^2H-nuclear magnetic resonance spin-lattice relaxation in cerebroside- and phospholipid-cholesterol bilayer membranes, Biophys. J. 54 (1988) 373–381.
[245] M. Auger, M.-R. van Calsteren, I.C.P. Smith, H.C. Jarrell, Glycerolipids: common features of molecular motion in bilayers, Biochemistry 29 (1990) 5815–5821.
[246] D.B. Fenske, K. Hamilton, H.C. Jarrell, E. Florio, K.R. Barber, C.W.M. Grant, Glycosphingolipids: ^2H NMR study of the influence of carbohydrate headgroup structure on ceramide acyl chain behavior in glycolipid-phospholipid bilayers, Biochemistry 30 (1991) 4503–4509.
[247] H.C. Jarrell, A.J. Wand, J.B. Giziewicz, I.C.P. Smith, The dependence of glyceroglycolipid orientation and dynamics on head group structure, Biochim. Biophys. Acta 897 (1987) 69–82.
[248] H.C. Jarrell, J.B. Giziewicz, I.C.P. Smith, Structure and dynamics of a glyceroglycolipid: a ^2H NMR study of head group orientation, ordering and effect on lipid aggregate structure, Biochemistry 25 (1986) 3950–3957.
[249] T. Bartels, R.S. Lankalapalli, R. Bittman, K. Beyer, M.F. Brown, Raftlike mixtures of sphingomyelin and cholesterol investigated by solid-state ^2H NMR spectroscopy, J. Am. Chem. Soc. 130 (2008) 14521–14532.
[250] S.L. Veatch, O. Soubias, S.L. Keller, K. Gawrisch, Critical fluctuations in domain-forming lipid mixtures, Proc. Natl. Acad. Sci. U.S.A. 104 (2007) 17650–17655.
[251] G.V. Martinez, E.M. Dykstra, S. Lope-Piedrafita, C. Job, M.F. Brown, NMR elastometry of fluid membranes in the mesoscopic regime, Phys. Rev. E 66 (2002) 050902-1–050902-4.
[252] G.V. Martinez, E.M. Dykstra, S. Lope-Piedrafita, M.F. Brown, Lanosterol and cholesterol-induced variations in bilayer elasticity probed by ^2H NMR relaxation, Langmuir 20 (2004) 1043–1046.
[253] G.W. Stockton, C.F. Polnaszek, A.P. Tulloch, F. Hasan, I.C.P. Smith, Molecular motion and order in single-bilayer vesicles and multilamellar dispersions of egg lecithin and lecithin-cholesterol mixtures. A deuterium nuclear magnetic resonance study of specifically labelled lipids, Biochemistry 15 (1976) 954–966.
[254] J.A. Urbina, S. Pekerar, H.-B. Le, J. Patterson, B. Montez, E. Oldfield, Molecular order and dynamics of phosphatidylcholine bilayer-membranes in the presence of cholesterol, ergosterol and lanosterol — a comparative study using ^2H-NMR, ^{13}C-NMR and ^{31}P-NMR spectroscopy, Biochim. Biophys. Acta 1238 (1995) 163–176.
[255] R. Jacobs, E. Oldfield, Deuterium nuclear magnetic resonance investigation of dimyristoyllecithin-dipalmitoyllecithin and dimyristoyllecithin–cholesterol mixtures, Biochemistry 18 (1979) 3280–3285.
[256] J. Forbes, C. Husted, E. Oldfield, High-field, high-resolution proton "magic-angle" sample-spinning nuclear magnetic resonance spectroscopic studies of gel and liquid crystalline lipid bilayers and the effects of cholesterol, J. Am. Chem. Soc. 110 (1988) 1059–1065.
[257] M.P.N. Gent, J.H. Prestegard, Cholesterol-phosphatidylcholine interactions in vesicle systems. Implication of vesicle size and proton magnetic resonance line-width changes, Biochemistry 13 (1974) 4027–4033.
[258] L. Miao, M. Nielsen, J. Thewalt, J.H. Ipsen, M. Bloom, M.J. Zuckermann, O.G. Mouritsen, From lanosterol to cholesterol: structural evolution and differential effects on lipid bilayers, Biophys. J. 82 (2002) 1429–1444.
[259] J.H. Ipsen, G. Karlström, O.G. Mouritsen, H. Wennerström, M.J. Zuckermann, Phase equilibria in the phosphatidylcholine–cholesterol system, Biochim. Biophys. Acta 905 (1987) 162–172.
[260] D. Marsh, Cholesterol-induced fluid membrane domains: a compendium of lipid-raft ternary phase diagrams, Biochim. Biophys. Acta 1788 (2009) 2114–2123.
[261] J. Aittoniemi, P.S. Niemelä, M.T. Hyvönen, M. Karttunen, I. Vattulainen, Insight into the putative specific interactions between cholesterol, sphingomyelin, and palmitoyl-oleoyl phosphatidylcholine, Biophys. J. 92 (2007) 1125–1137.
[262] F.M. Goñi, A. Alonso, L.A. Bagatolli, R.E. Brown, D. Marsh, M. Prieto, J.L. Thewalt, Phase diagrams of lipid mixtures relevant to the study of membrane rafts, Biochim. Biophys. Acta 1781 (2008) 665–684.
[263] S.L. Veatch, I.V. Polozov, K. Gawrisch, S.L. Keller, Liquid domains in vesicles investigated by NMR and fluorescence microscopy, Biophys. J. 86 (2004) 2910–2922.
[264] C. Hofsass, E. Lindahl, O. Edholm, Molecular dynamics simulations of phospholipid bilayers with cholesterol, Biophys. J. 84 (2003) 2192–2206.
[265] J.L. Thewalt, M. Bloom, Phosphatidylcholine: cholesterol phase diagrams, Biophys. J. 63 (1992) 1176–1181.
[266] G.W. Feigenson, J.T. Buboltz, Ternary phase diagram of dipalmitoyl-PC/dilauroyl-PC/cholesterol: nanoscopic domain formation driven by cholesterol, Biophys. J. 80 (2001) 2775–2788.
[267] G.W. Feigenson, Phase behavior of lipid mixtures, Nat. Chem. Biol. 2 (2006) 560–563.
[268] A. Seelig, J. Seelig, Bilayers of dipalmitoyl-3-*sn*-phosphatidylcholine. Conformational differences between the fatty acyl chains, Biochim. Biophys. Acta 406 (1975) 1–5.
[269] E.J. Dufourc, E.J. Parish, S. Chitrakorn, I.C.P. Smith, Structural and dynamical details of cholesterol–lipid interaction as revealed by deuterium NMR, Biochemistry 23 (1984) 6062–6071.
[270] G.W. Stockton, I.C.P. Smith, A deuterium nuclear magnetic resonance study of the condensing effect of cholesterol on egg phosphatidylcholine bilayer membranes. I. Perdeuterated fatty acid probes, Chem. Phys. Lipids 17 (1976) 251–263.
[271] A. Blume, R.J. Wittebort, S.K. Das Gupta, R.G. Griffin, Phase equilibria, molecular conformation, and dynamics in phosphatidylcholine/phosphatidylethanolamine bilayers, Biochemistry 21 (1982) 6243–6253.
[272] P.R. Cullis, P.W.M. van Dijck, B. de Kruijff, J. de Gier, Effects of cholesterol on the properties of equimolar mixtures of synthetic phosphatidylethanolamine and phosphatidylcholine. A ^{31}P-NMR and differential scanning calorimetry study, Biochim. Biophys. Acta 513 (1978) 21–30.
[273] C.P.S. Tilcock, M.B. Bally, S.B. Farren, P.R. Cullis, Influence of cholesterol on the structural preferences of dioleoylphosphatidylethanolamine-dioleoylphosphatidylcholine systems: a phosphorus-31 and deuterium nuclear magnetic resonance study, Biochemistry 21 (1982) 4596–4601.
[274] M.F. Brown, J. Seelig, Influence of cholesterol on the polar region of phosphatidylcholine and phosphatidylethanolamine bilayers, Biochemistry 17 (1978) 381–384.
[275] P.W.M. van Dyck, B. de Kruijff, L.L.M. van Deenen, J. de Gier, R.A. Demel, The preference of cholesterol for phosphatidylcholine in mixed phosphatidylcholine-phosphatidylethanolamine bilayers, Biochim. Biophys. Acta 455 (1976) 576–587.
[276] R. Ghosh, J. Seelig, The interaction of cholesterol with bilayers of phosphatidylethanolamine, Biochim. Biophys. Acta 691 (1982) 151–160.
[277] A. Blume, D.M. Rice, R.J. Wittebort, R.G. Griffin, Molecular dynamics and conformation in the gel and liquid-crystalline phases of phosphatidylethanolamine bilayers, Biochemistry 21 (1982) 6220–6230.
[278] T.P. Trouard, A.A. Nevzorov, T.M. Alam, C. Job, J. Zajicek, M.F. Brown, Influence of cholesterol on dynamics of dimyristoylphosphatidylcholine as studied by deuterium NMR relaxation, J. Chem. Phys. 110 (1999) 8802–8818.

[279] G. Lindblom, L.B.-Å. Johansson, G. Arvidson, Effect of cholesterol in membranes. Pulsed nuclear magnetic resonance measurements of lipid lateral diffusion, Biochemistry 20 (1981) 2204–2207.
[280] G.P. Holland, T.M. Alam, Multi-dimensional ^{1}H–^{13}C HETCOR and FSLG-HETCOR NMR study of sphingomyelin bilayers containing cholesterol in the gel and liquid crystalline states, J. Magn. Reson. 181 (2006) 316–326.
[281] R.M. Epand, R.F. Epand, Non-raft forming sphingomyelin cholesterol mixtures, Chem. Phys. Lipids 132 (2004) 37–46.
[282] R. Epand, Cholesterol in bilayers of sphingomyelin or dihydrosphingomyelin at concentrations found in ocular lens membranes, Biophys. J. 84 (2003) 3102–3110.
[283] Y. Barenholz, T.E. Thompson, Sphingomyelin: biophysical aspects, Chem. Phys. Lipids 102 (1999) 29–34.
[284] B. Snyder, E. Freire, Compositional domain structure in phosphatidylcholine–cholesterol and sphingomyelin–cholesterol bilayers, Proc. Natl. Acad. Sci. U.S.A. 77 (1980) 4055–4059.
[285] A. Tsamaloukas, H. Szadkowska, H. Heerklotz, Thermodynamic comparison of the interactions of cholesterol with unsaturated phospholipid and sphingomyelins, Biophys. J. 90 (2006) 4479–4487.
[286] C. Kan, R. Bittman, J. Hadju, Phospholipids containing nitrogen- and sulfur-linked chains: kinetics of cholesterol exchange between vesicles, Biochim. Biophys. Acta 1066 (1991) 95–101.
[287] W. Gou, V. Kurze, T. Huber, N.H. Afdhal, K. Beyer, J.A. Hamilton, A solid-state NMR study of phospholipid–cholesterol interactions: sphingomyelin–cholesterol binary systems, Biophys. J. 83 (2002) 1465–1478.
[288] F. Aussenac, M. Tavares, E.J. Dufourc, Cholesterol dynamics in membranes of raft composition: a molecular point of view from ^{2}H and ^{31}P solid-state NMR, Biochemistry 42 (2003) 1383–1390.
[289] A. Bunge, P. Müller, M. Stöckl, A. Herrmann, D. Huster, Characterization of the ternary mixture of sphingomyelin, POPC, and cholesterol: support for an inhomogeneous lipid distribution at high temperatures, Biophys. J. 94 (2008) 2680–2690.
[290] R.F.M. De Almeida, L.M.S. Loura, M. Prieto, Membrane lipid domains and rafts: current applications of fluorescence lifetime spectroscopy and imaging, Chem. Phys. Lipids 157 (2009) 61–77.
[291] J. Yuan, A. Kiss, Y.H. Pramudya, L.T. Nguyen, L.S. Hirst, Solution synchotron X-ray diffraction reveals structural details of lipid domains in ternary mixtures, Phys. Rev. E 79 (2009) 031924-1–031924-9.
[292] P.J. Quinn, C. Wolf, Hydrocarbon chains dominate coupling and phase coexistence in bilayers of natural phosphatidylcholines and sphingomyelins, Biochim. Biophys. Acta 1788 (2009) 1126–1137.
[293] E. van den Brink-van der Laan, J.A. Killian, B. de Kruijff, Nonbilayer lipids affect peripheral and integral membrane proteins via changes in the lateral pressure profile, Biochim. Biophys. Acta 1666 (2004) 275–288.
[294] P.K.J. Kinnunen, A. Kõiv, J.Y.A. Lehtonen, M. Rytömaa, P. Mustonen, Lipid dynamics and peripheral interactions of proteins with membrane surfaces, Chem. Phys. Lipids 73 (1994) 181–207.
[295] S.J. Opella, C. Ma, F.M. Marassi, Nuclear magnetic resonance of membrane-associated peptides and proteins, Meth. Enzymol. 339 (2001) 285–313.
[296] S.H. White, W.C. Wimley, Membrane protein folding and stability: physical principles, Annu. Rev. Biophys. Biomol. Struct. 28 (1999) 319–365.
[297] T.A. Cross, S.J. Opella, Solid-state NMR structural studies of peptides and proteins in membranes, Curr. Opin. Struct. Biol. 4 (1994) 574–581.
[298] D. Otten, M.F. Brown, K. Beyer, Softening of membrane bilayers by detergents elucidated by deuterium NMR spectroscopy, J. Phys. Chem. B 104 (2000) 12119–12129.
[299] D. Otten, K. Beyer, Chain length mismatch and packing constraints of free fatty acids in a hexagonal detergent host phase. A wide line deuterium NMR study, Chem. Phys. Lipids 77 (1995) 203–215.
[300] R.L. Thurmond, D. Otten, M.F. Brown, K. Beyer, Structure and packing of phosphatidylcholines in lamellar and hexagonal liquid-crystalline mixtures with a nonionic detergent: a wide-line deuterium and phosphorus-31 NMR study, J. Phys. Chem. 98 (1994) 972–983.
[301] K. Beyer, A ^{31}P- and ^{2}H-NMR study on lecithins in liquid crystalline polyoxyethylene, Chem. Phys. Lipids 34 (1983) 65–80.
[302] G. Klose, B. Mädler, H. Schäfer, K. Schneider, Structural characterization of POPC and $C_{12}E_4$ in their mixed membranes at reduced hydration by solid-state ^{2}H NMR, J. Phys. Chem. B 103 (1999) 3022–3029.
[303] G. Klose, S. Eisenblätter, B. König, Ternary phase diagram of mixtures of palmitoyl-oleoyl phosphatidylcholine, tetraoxyethylene dodecyl ether and heavy water as seen by ^{31}P and ^{2}H NMR, J. Colloid Interface Sci. 172 (1995) 438–446.
[304] U. Henriksson, M. Jonströmer, U. Olsson, O. Söderman, G. Klose, ^{2}H NMR study of molecular dynamics and organization in the system $C_{12}E_4$-water, J. Phys. Chem. 95 (1991) 3815–3819.
[305] D. Otten, L. Löbbecke, K. Beyer, Stages of the bilayer-micelle transition in the system phosphatidylcholine-$C_{12}E_8$ as studied by deuterium- and phosphorous-NMR, light scattering, and calorimetry, Biophys. J. 68 (1995) 584–597.
[306] E. London, G.W. Feigenson, Phosphorus NMR analysis of phospholipids in detergents, J. Lipid Res. 20 (1979) 408–412.
[307] D. Huster, L. Xiao, M. Hong, Solid-state NMR investigation of the dynamics of the soluble and membrane-bound colicin Ia channel-forming domain, Biochemistry 40 (2001) 7662–7674.
[308] R.M. Epand, H.J. Vogel, Diversity of antimicrobial peptides and their mechanisms of action, Biochim. Biophys. Acta 1462 (1999) 11–28.
[309] J.A. Killian, F. Borle, B. de Kruijff, J. Seelig, Comparative ^{2}H- and ^{31}P-NMR study of the properties of palmitoyllysophosphatidylcholine in bilayers with gramicidin, cholesterol and dipalmitoylphosphatidylcholine, Biochim. Biophys. Acta 854 (1986) 133–142.
[310] R.M. Epand, Fusion peptides and the mechanism of viral fusion, Biochim. Biophys. Acta 1614 (2003) 116–121.
[311] B. Nuscher, F. Kamp, T. Mehnert, S. Odoy, C. Haass, P.J. Kahle, K. Beyer, Alpha-synuclein has a high affinity for packing defects in a bilayer membrane: a thermodynamics study, J. Biol. Chem. 279 (2004) 21966–21975.
[312] T. Bartels, L.S. Ahlstrom, A. Leftin, F. Kamp, C. Haass, M.F. Brown, K. Beyer, The N-terminus of the intrinsically disordered protein α-synuclein triggers membrane binding and helix folding, Biophys. J. 99 (2010) 2116–2124.
[313] E. Perozo, A. Kloda, D.M. Cortes, B. Martinac, Physical principles underlying the transduction of bilayer deformation forces during mechanosensitive channel gating, Nat. Struct. Biol. 9 (2002) 696–703.
[314] C. Husted, B. Montez, C. Le, M.A. Moscarello, E. Oldfield, Carbon-13 "magic-angle" sample-spinning nuclear magnetic resonance studies of human myelin, and model membrane systems, Magn. Reson. Med. 29 (1993) 168–178.
[315] J. Forbes, J. Bowers, X. Shan, L. Moran, E. Oldfield, M.A. Moscarello, Some new developments in solid-state nuclear magnetic resonance spectroscopic studies of lipids and biological membranes, including the effects of cholesterol in model and natural systems, J. Chem. Soc. Faraday Trans. I 84 (1988) 3821–3849.
[316] F. Millett, P.A. Hargrave, M.A. Raftery, Natural abundance ^{13}C nuclear magnetic resonance spectra of the lipid in intact bovine retinal rod outer segment membranes, Biochemistry 12 (1973) 3591–3592.
[317] M.F. Brown, G.P. Miljanich, E.A. Dratz, Proton spin-lattice relaxation of retinal rod outer segment membranes and liposomes of extracted phospholipids, Proc. Natl. Acad. Sci. U.S.A. 74 (1977) 1978–1982.
[318] M.F. Brown, G.P. Miljanich, E.A. Dratz, Interpretation of 100- and 360-MHz proton magnetic resonance spectra of retinal rod outer segment disk membranes, Biochemistry 16 (1977) 2640–2648.
[319] M.F. Brown, A.J. Deese, E.A. Dratz, Proton, carbon-13, and phosphorus-31 NMR methods for the investigation of rhodopsin–lipid interactions in retinal rod outer segment membranes, Meth. Enzymol. 81 (1982) 709–728.
[320] M.F. Brown, G.P. Miljanich, L.K. Franklin, E.A. Dratz, ^{1}H-NMR studies of protein–lipid interactions in retinal rod outer segment disc membranes, FEBS Lett. 70 (1976) 56–59.
[321] A.J. Deese, E.A. Dratz, M.F. Brown, Retinal rod outer segment lipids form bilayers in the presence and absence of rhodopsin: a ^{31}P NMR study, FEBS Lett. 124 (1981) 93–99.
[322] L.C.P.J. Mollevanger, E.A. Dratz, B. de Kruijff, C.W. Hilbers, W.J. de Grip, ^{31}P-NMR investigation of magnetically oriented rod outer segments. Spectral analysis and identification of individual phospholipids, Eur. J. Biochem. 156 (1986) 383–390.
[323] O. Soubias, W.E. Teague, K. Gawrisch, Evidence for specificity in lipid–rhodopsin interactions, J. Biol. Chem. 281 (2006) 33233–33241.
[324] A.C. McLaughlin, L. Herbette, J.K. Blaise, C.T. Wang, L. Hymel, S. Fleischer, ^{31}P-NMR studies of oriented multilayers formed from isolated sarcoplasmic reticulum and reconstituted sarcoplasmic reticulum. Evidence that "boundary-layer" phospholipid is not immobilized, Biochim. Biophys. Acta 643 (1981) 1–16.
[325] J.D. Robinson, N.J.M. Birdsall, A.G. Lee, J.C. Metcalfe, ^{13}C and ^{1}H nuclear magnetic resonance relaxation measurements of the lipids of sarcoplasmic reticulum membranes, Biochemistry 11 (1972) 2903–2909.
[326] J.F. Ellena, R.D. Pates, M.F. Brown, ^{31}P NMR spectra of rod outer segment and sarcoplasmic reticulum membranes show no evidence of immobilized components due to lipid–protein interactions, Biochemistry 25 (1986) 3742–3748.
[327] A.J. Deese, E.A. Dratz, F.W. Dahlquist, M.R. Paddy, Interaction of rhodopsin with two unsaturated phosphatidylcholines: a deuterium NMR study, Biochemistry 20 (1981) 6420–6427.
[328] A.D. Albert, S.A. Lane, P.L. Yeagle, ^{2}H and ^{31}P nuclear magnetic resonance studies of membranes containing bovine rhodopsin, J. Membr. Biol. 87 (1985) 211–215.
[329] O. Soubias, W.E. Teague, K.G. Hines, D.C. Mitchell, K. Gawrisch, Contribution of membrane elastic energy to rhodopsin function, Biophys. J. 99 (2010) 817–824.
[330] M. Kobayashi, A.V. Struts, T. Fujiwara, M.F. Brown, H. Akutsu, Fluid mechanical matching of H^{+}-ATP synthase subunit *c*-ring with lipid membranes revealed by ^{2}H solid-state NMR, Biophys. J. 94 (2008) 4339–4347.
[331] D. Lingwood, K. Simons, Lipid rafts as a membrane-organizing principle, Science 327 (2010) 46–50.